Tidal Exchange through the Kuril Straits

TOMOHIRO NAKAMURA, TOSHIYUKI AWAJI, TAKAKI HATAYAMA, AND KAZUNORI AKITOMO

Department of Geophysics, Kyoto University, Kyoto, Japan

TAKATOSHI TAKIZAWA

Japan Marine Science and Technology Center, Yokosuka, Japan

(Manuscript received 11 August 1998, in final form 19 July 1999)

ABSTRACT

The tidal exchange between the Okhotsk Sea and the North Pacific Ocean is studied numerically with particular emphasis on the predominant K_1 barotropic component. The calculated harmonic constants of the K_1 tide in and around the Okhotsk Sea agree well with those obtained from extensive tide gauge observations. The features of the simulated tidal fields are similar to those reported in the literature. Since the K_1 tide is subinertial in the Okhotsk Sea, topographically trapped waves are effectively generated, contributing to strong tidal currents with a maximum amplitude of over 1.5 m s^{-1} in the Kuril Straits. The structures of tide-induced mean flows in most passages of the straits are characterized by ''bidirectional currents'' (in which the mean flow exhibits a reversal in direction across the passages). This feature is clearly indicated in NOAA infrared imagery. The mean transport shows significant net exchange of water via several straits in the Kuril Islands. A transport of about 5.0 Sv (1 Sv $\equiv 10^6$ m^3 s^{-1}) toward the North Pacific is produced by the K_1 tide, primarily through the Bussol, Kruzenshterna, and Chetverty Straits. Analysis reveals that the bidirectional mean currents at shallow passages are produced through the well-known process of tidal rectification over variable bottom topography, whereas in deep passages such as Bussol Strait, propagating trapped waves along the islands are essential for generating the bidirectional mean currents. Particle tracking clearly demonstrates these features. The tidal current is therefore thought to play a major role in water exchange processes between the Okhotsk Sea and the North Pacific.

1. Introduction

The Okhotsk Sea (Fig. 1) is separated from the northwestern Pacific Ocean by the Kuril Islands and the sills in the straits, almost all of which are shallower than 600 m except for the Bussol (~2200 m) and Kruzenshterna (~1500 m) Straits. However, the transport process between the Okhotsk Sea and the North Pacific Ocean plays an important role not only in the local environment but also in determining the water properties of the North Pacific. The North Pacific is the source of most of the water in the Okhotsk Sea. This inflow is thought to take place mainly through the northern part of the Kuril Straits, whose neighborhood remains ice free even in the most severe winters (Reid 1965; Kawasaki and Kono 1994).

The Okhotsk Sea, on the other hand, is thought to have a significant impact upon the North Pacific. Previous studies in the northwest Pacific found that a plume of low salinity water at 27.0 σ_θ extended to the south from the Kuril Straits and that the confluence of the East Kamchatka Current and the discharge from the Okhotsk Sea forms both the Oyashio current, which flows along the Kuril Islands as part of the western boundary current of the subarctic gyre, and the Subarctic Current to the east, thus indicating that the Okhotsk Sea is the most likely source of low salinity water in the North Pacific (Wüst 1930; Favorite et al. 1976; Talley 1991). Kitani (1973) showed that in the northern Okhotsk Sea, the freezing of fresh surface waters can form cold saline waters as dense as 27.05 σ_θ, which still have lower salinity than the ambient waters at the same density. By relating an analysis of historical hydrographic data to Kitani's (1973) result, Talley (1991) proposed that the North Pacific at mid depth is ventilated through sea ice formation in the innermost part of the Okhotsk Sea and local vertical mixing in the Kuril Straits. From potential vorticity maps, Talley (1993) and Yasuda et al. (1996) commented that the Okhotsk Sea supplies low salinity water to the North Pacific Intermediate Water (NPIW) characterized by a salinity minimum centered at 26.8 σ_θ. These conclusions were also confirmed by recent studies. Warner et al. (1996) showed that the Okhotsk Sea is an important location for the ventilation of the intermediate water of the North Pacific based on chlo-

Corresponding author address: Dr. Tomohiro Nakamura, Department of Geophysics, Kyoto University, Kyoto 606 8502, Japan.
E-mail: nakamura@kugi.kyoto-u.ac.jp

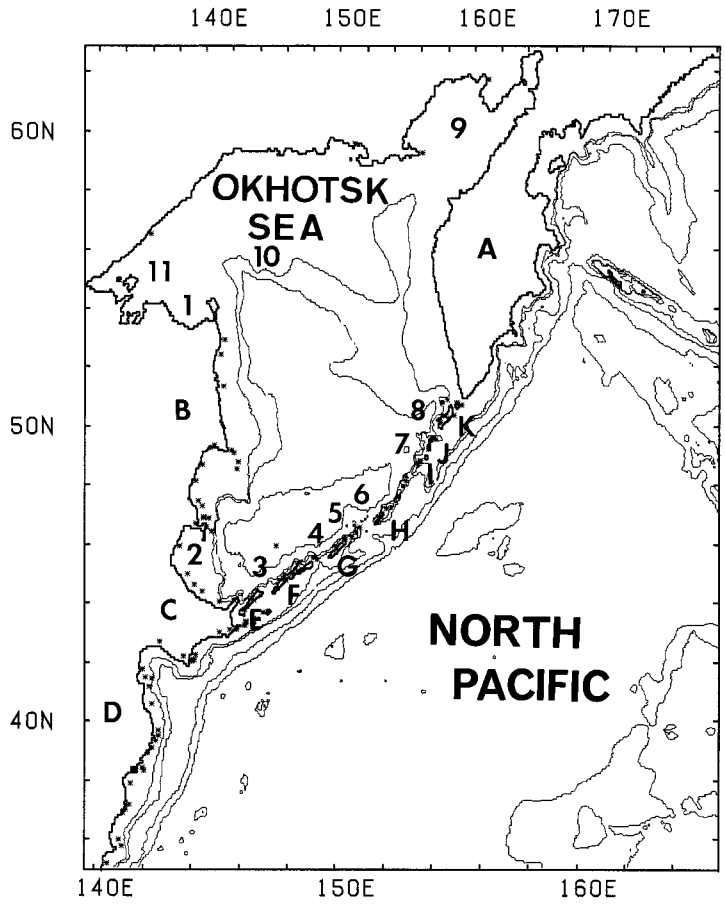

No.	Straits and Bays	No.	Islands
1:	Tartar St.	A:	Kamchatka Pen.
2:	Soya St.	B:	Sakhalin Isl.
3:	Kunashiri St.	C:	Hokkaido
4:	Etrofu St.	D:	Honshu
5:	Urup St.	E:	Kunashiri Isl.
6:	Bussol St.	F:	Etrofu Isl.
7:	Kruzenshterna St.	G:	Urup Isl.
8:	Chetverty St.	H:	Simusir Isl.
9:	Shelikova Bay	I:	Shiashikotan Isl.
10:	Kashebarova Bank	J:	Onekotan Isl.
11:	Shantarsky Bay	K:	Paramusir Isl.

FIG. 1. Model domain and topography. Contours are at 500, 1000, 3000, and 5000 m. Symbols denote tide gauge locations for the International Hydrographic Office (IHO) tidal harmonic constants edited by the Canadian Department of Fisheries and Oceans.

rofluorocarbons (CFCs) observations. Yasuda (1997) showed the presence of a pycnostad (i.e., a region of low potential vorticity) at 26.8 σ_θ in the Okhotsk Sea and concluded that the low potential vorticity water flowing out into the North Pacific determines even the density of the NPIW. Thus, a clarification of the exchange processes through the Kuril Straits is indispensable for a better understanding of water mass formation in the North Pacific (such as the NPIW).

Past studies regarded the current in the Okhotsk Sea as part of the cyclonic subarctic circulation, which predominantly flows into the Okhotsk Sea through Kruzenshterna Strait and out through Bussol Strait. However, recent observational studies suggest that there is great difficulty in explaining this in/outflow in terms of geostrophic balance. One reason for this is that the overall surface dynamic height is higher in the Okhotsk Sea than in the northwestern North Pacific (Kawasaki and Kono 1992). Another reason is that due to the weak stratification, the Oyashio extends to such depths that it tends to flow along the continental shelf slope along the Kuril Islands (2000~3000 m deep) and is most likely unable to pass over the shallow sills in the Kuril Straits. In fact, Stabeno et al. (1994) reported that only 1 of the 14 buoys that were transported along the Kuril Islands entered the Okhotsk Sea. This indicates that the Oyashio does not directly flow into and out of the Okhotsk Sea. Moreover, Leonov (1960) and Moroshkin (1966) mentioned that bidirectional currents occur in most passages. This picture is clearly seen in the *NOAA-12* advanced very high-resolution radiometer imagery (Fig. 2). Such current structure cannot be explained by large-scale wind-driven geostrophic flow.

These observational results strongly suggest the importance of nongeostrophic components. In fact, tidal currents, especially diurnal, are dominant in and around the Kuril Straits (e.g., Thomson et al. 1996), and their speeds reach a few knots. According to previous studies on tidal exchange (e.g., Huthnance 1973; Zimmerman 1978; Awaji et al. 1980; Robinson 1981), such strong tidal currents are expected to induce significant mean transport, even if there are sills in the straits. Moreover, tide-induced mean currents allow us to explain the bidirectional structure of the (local) mean currents in the passages.

Suzuki and Kanari (1986) performed a simulation of

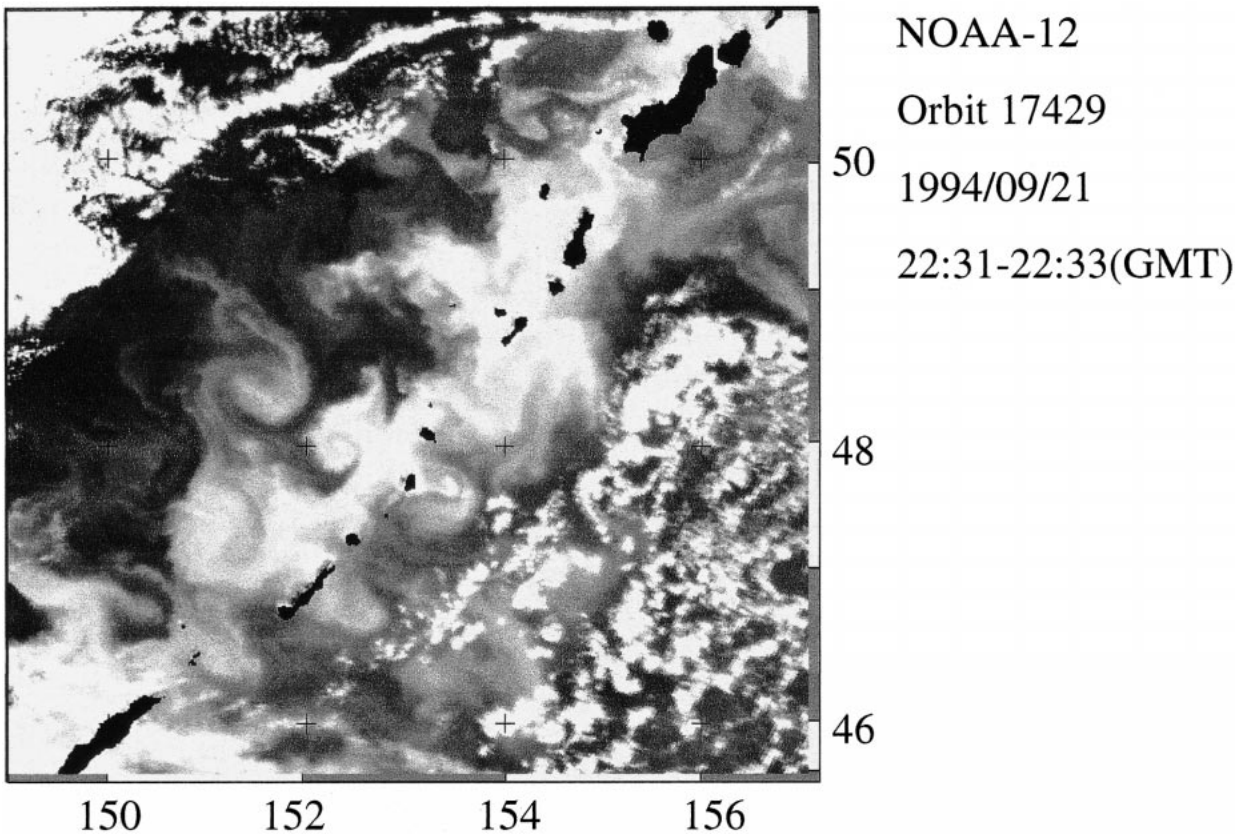

FIG. 2. Infrared image of the Kuril Straits taken from the *NOAA-12* satellite on 21 September 1994. (Figure courtesy of Prof. S. Saitoh)

the tidal field in the Okhotsk Sea and showed that in the Okhotsk Sea, 1) the K_1 tide is dominant, M_2 is second, and the O_1 component the third largest in elevation amplitude; 2) diurnal tides propagate from east to west and have two amphidromic like points near the Soya and Nemuro Straits; and 3) the semidiurnal tides are propagating waves with two amphidromic points. Though they provided many interesting results, the tidal currents around the straits were not reproduced in sufficiently detailed structure or accuracy since Suzuki and Kanari (1986) did not aim at estimating the transport through the Kuril Straits.

Thus, as a first step toward understanding the transport process and estimating its magnitude, we have investigated numerically the characteristics of the barotropic tides and tidal currents around the Okhotsk Sea. Investigation of barotropic tides may be a meaningful first step since stratification in and around the Okhotsk Sea is weak. We have then estimated the mean transport through the Kuril Straits and identified the mechanism of tidal exchange. In this paper, though numerical simulations for the K_1, O_1, P_1, M_2, and S_2 tides have been successfully performed, we discuss our result with a particular focus on the predominant component, the barotropic K_1 tide. The dynamics of other diurnal tides are almost the same as that of the K_1 tide. Because semidiurnal tides are considerably smaller than the diurnal tides in current speed, we describe the M_2 tide only. Section 2 of this paper describes the numerical model. Section 3 is devoted to a description of the characteristics of the calculated K_1 and M_2 tidal fields and their comparison with tide gauge observations. In section 4, tidal exchange is estimated from the Eulerian point of view and the mechanism causing the transport is investigated in section 5. The results are discussed in section 6 and are summarized in section 7.

2. Model

The model region shown in Fig. 1 covers the entire Okhotsk Sea and part of the North Pacific. The open boundaries are set away from the Okhotsk Sea in order to reproduce tidal wave propagation from the North Pacific, which is one of the major forcing factors for the tidal motion around the Okhotsk Sea, and to prevent the influence of artificial disturbances generated at the open boundaries on the tidal field around the Kuril Straits. Since past studies on tidal current dynamics suggest that tidal currents near straits (including the Kuril Straits) are greatly influenced by topographic features, we resolved the topography of the model region in greater detail. Using the DBDB5 topographic data (National

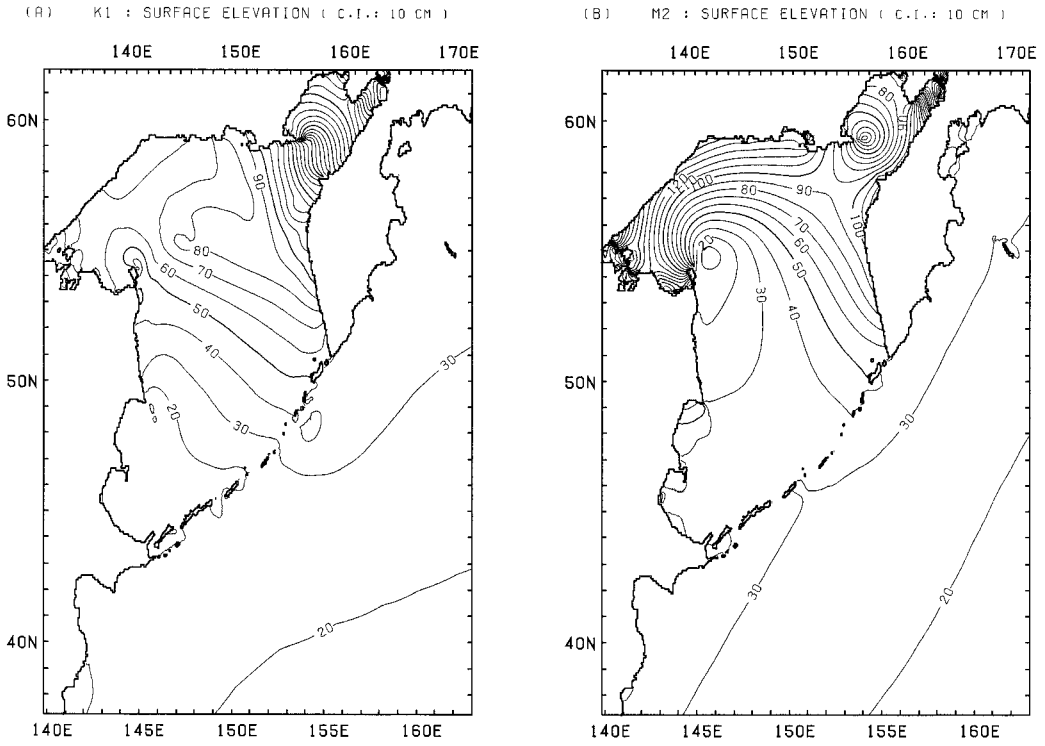

FIG. 3. Calculated coamplitude lines of tidal elevation for (a) the K_1 tide and (b) the M_2 tide. The contour interval is 10 cm.

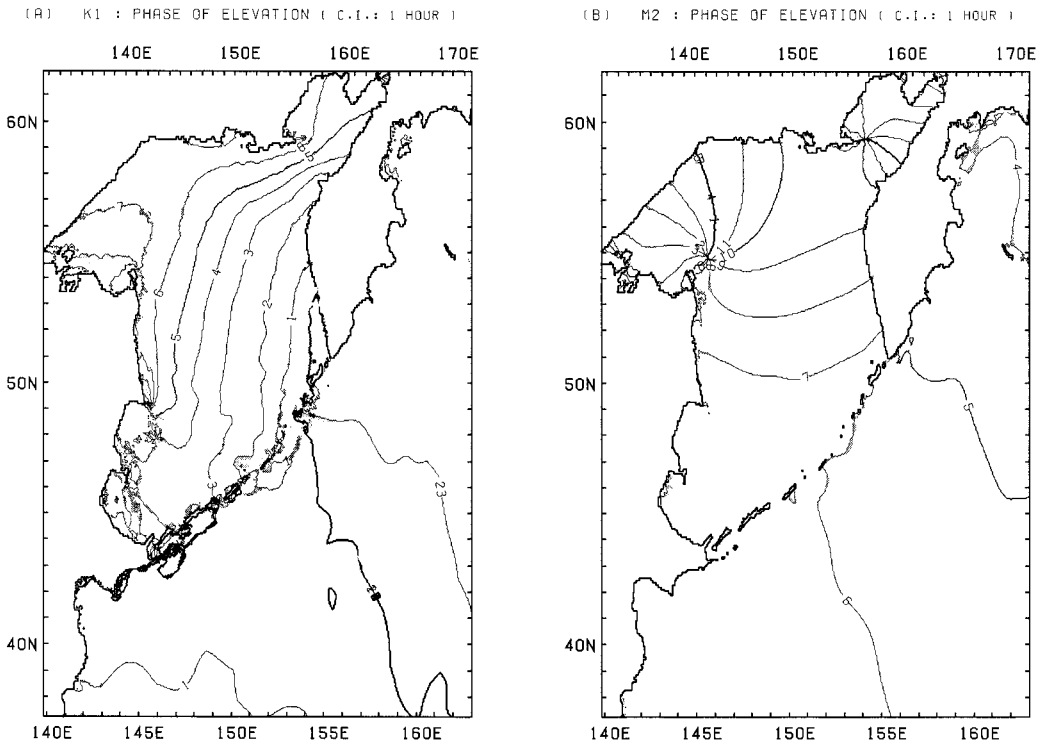

FIG. 4. Calculated cophase lines of tidal elevation for (a) the K_1 tide and (b) the M_2 tide. The contour intervals are 1 lunar hour.

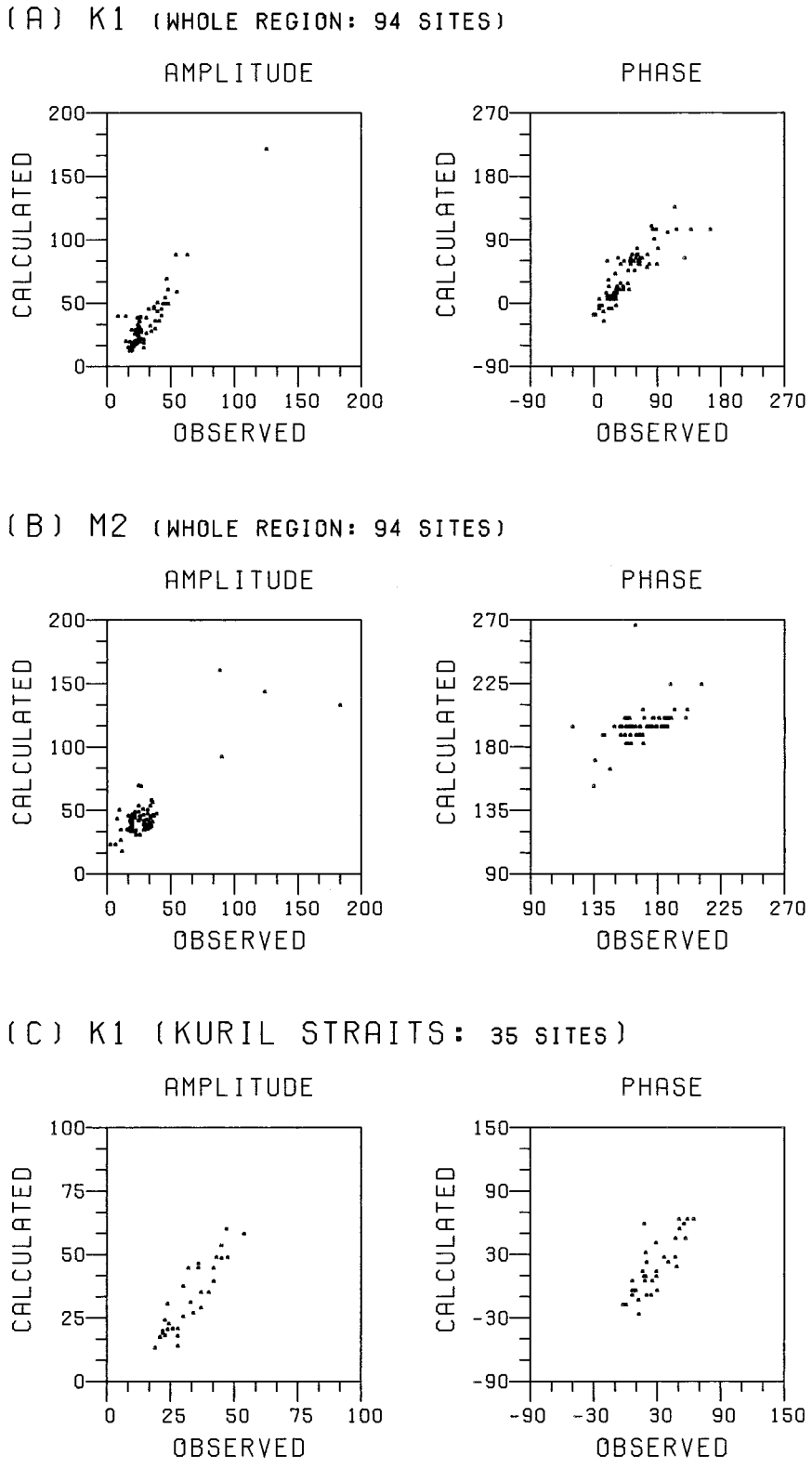

FIG. 5. The correlation coefficients between model results and observed harmonic constants for (a) the K_1 tide, (b) the M_2 tide, and (c) the K_1 tide (for the Kuril Straits only).

Geophysical Data Center, Boulder, Colorado), the model domain is divided into 5 km × 5 km grids.

The numerical model is the same as that used by Hatayama et al. (1996), with the familiar barotropic tidal equations given as

$$\frac{\partial \mathbf{u}}{\partial t} + (\mathbf{u} \cdot \nabla)\mathbf{u} + f\mathbf{k} \times \mathbf{u} = -g\nabla(\alpha_0 \eta - \beta_0 \zeta) + A_H \nabla^2 \mathbf{u} - \frac{\kappa \mathbf{u}|\mathbf{u}|}{H + \eta}, \quad (1)$$

$$\frac{\partial \eta}{\partial t} + \nabla \cdot [(H + \eta)\mathbf{u}] = 0, \quad (2)$$

where (x, y) are eastward and northward coordinates; t is time; $\eta(x, y, t)$ is the surface elevation, $\zeta(x, y, t)$ is the equilibrium tide describe below; $\mathbf{u}(x, y, t)$ is the horizontal velocity vector; H is the depth; $f = f_0 + \beta y$ ($\beta = 2.28 \times 10^{-13}$ cm^{-1} s^{-1}) is the Coriolis parameter; g is the gravity acceleration; κ is the bottom friction coefficient; and A_H is the horizontal eddy viscosity coefficient. It should be noted that the scheme used in this model conserves both mass and enstrophy, as recommended by Huthnance (1981), in order to prevent spurious contributions to the torque balance, which determines the residual current strength.

The parameters α_0 and β_0 account for the effect of the tidal potentials, earth tide, and loading tide. Here we set $\alpha_0 = 0.900$, $\beta_0 = 0.690$ for the K_1 component according to Schwiderski (1980). Although the TOPEX/POSEIDON Satellite Tidal Committee recommends somewhat difference values of $\alpha_0 = 0.940$ and $\beta_0 = 0.736$, the former values give better agreement with the observations.

The equilibrium tide ζ is expressed as

$$\zeta = K \sin 2\phi \cos(\sigma t + \lambda) \quad (3)$$

for diurnal and

$$\zeta = K \cos^2 \phi \cos(\sigma t + 2\lambda) \quad (4)$$

for semidiurnal tides, where K and σ are the amplitude and frequency taken from Schwiderski (1980), and λ and ϕ are longitude and latitude, respectively. The astronomical arguments are neglected since tidal fields are calculated for each tidal component.

The bottom stress is added via a quadratic law with $\kappa = 0.0026$. This formulation makes it possible for the bottom stress to generate relative vorticity around the straits as described in section 4 (the dependency on this friction scheme will be discussed in section 7). In the determination of the horizontal eddy viscosity coefficient A_H, we used the formulation by Schwiderski (1980) in which A_H depends linearly on the horizontal and vertical mixing lengths as

$$A_H(x, y) = a_h \Delta L H(x, y), \quad (5)$$

where ΔL is the grid length (constant in this model) and a_h the reduced eddy coefficient determined to be 7.5×10^{-6} (s^{-1}) by trial and error to achieve the best agreement with observations. This value gives $A_H = 7.5 \times 10^5$ cm^2 s^{-1} at 2000-m depth.

The boundary conditions are set as follows. A no-slip condition is imposed at the land boundaries. At the open boundaries, the tidal elevation is specified using the results of Schwiderski (1979, 1981) with the exceptions of the Soya and Tartar Straits, where it is given from tide gauge observations near the open boundaries. Thus, the model is forced by these boundary oscillations in addition to the effects of the tide generating potential, the earth tide, and the ocean loading tide. To reduce artificial disturbances at open boundaries due to wave reflection, Orlanski's (1976) radiation condition for velocity is used together with the sponge zone condition within 5 grid points from the open boundaries where A_H is amplified linearly.

The initial conditions are zero currents and a flat sea surface. We performed 24 cycles of the integration for each tidal component, by which time the model ocean reached an almost steady oscillation and the final cycle of simulation is used for the analysis described below.

3. Tidal fields in the Okhotsk Sea

The harmonic constants (sea-level amplitude and phase) are calculated at every grid point, and the spatial distributions of the coamplitude and cophase lines for K_1 and M_2 tides are shown in Figs. 3 and 4, respectively. These distributions are qualitatively consistent with previous studies (Ogura 1923; Suzuki and Kanari 1986; Mazzega and Bérge 1994). To estimate water exchange quantitatively, a more stringent check on our model result is required. Thus we made a comparison with the International Hydrographic Office (IHO) tidal harmonic constants, the locations of which are shown in Fig. 1.

For the predominant K_1 tide component, the correlation coefficients between the calculated and the observed harmonic constants are high (0.904 for phase and 0.976 for amplitude) in the whole region (Fig. 5a). Although the amplitudes at a few sites are overestimated compared with the observational values, the points with the largest discrepancies are around the northern coast of the Okhotsk Sea and the overestimate is insignificant in other regions. The correlation coefficients for data in the Kuril Straits only are somewhat lower (0.814 for phase and 0.907 for amplitude in Fig. 5c) than those for the whole region, but still remain high.

Further, we estimate the root mean square (rms) error of the calculated K_1 tide over the entire region from the expression

$$\mathrm{RMS} = \frac{1}{N}\sum^{N}\frac{1}{T}\left[\int_0^T \{A_M\cos(\sigma t - P_M) - A_O\cos(\sigma t - P_O)\}^2\,dt\right]^{1/2}, \quad (6)$$

where N is the total number of tide gauge observations, T is the tidal periods, σ the frequency, A and P the amplitude and phase, respectively, and the suffixes M and O denote the calculated and observed harmonic constants, respectively. The calculated rms error is 8.06 cm over the whole region and 6.75 cm in the Kuril Straits.

Owing to the lack of current measurements, we can compare the model results with observation only in elevation data. Although it is not safe to assume that good correlation with elevation data implies good model estimates of currents, we believe that, at least qualitatively, the features of current field are well reproduced. In a quantitative sense, the current field is probably underestimated as will be discussed in section 7.

For the M_2 tide, the correlation coefficients (Fig. 5b) are also high (0.825 for amplitude and 0.929 for phase). The calculated rms error is 12.39 cm, since the amplitude is slightly overestimated. Most of the sites with significant discrepancies in amplitude are located in Shantarsky and Shelikova Bays in the northern Okhotsk Sea, where complicated coastlines are not sufficiently resolved. When the data at such sites are removed, the rms error becomes 9.5 cm. Thus it can be said that the calculated M_2 tidal field is similar to that observed.

The K_1 tide is the largest component in elevation amplitude in the eastern Okhotsk Sea. From Fig. 4a, it can be seen that the K_1 tidal field in the Okhotsk Sea is mostly determined by the tidal wave coming from the North Pacific, which enters the Okhotsk Sea mainly through the northeastern part of the Kuril Straits. These waves progress directly in a roughly westward direction and along the coast in a cyclonic fashion, and an amphidromic-like point appears on the east coast of Sakhalin. Around the Kuril Straits, cophase lines are complicated because of wave trapping along the islands. The elevation amplitude is large at the northeastern part of the straits and, in general, increases with decreasing depth toward the northern part of the Okhotsk Sea, with a local maximum of about 0.8 m near the Kushevarova Bank. In Shelikhova Bay, located in the northeast of the Okhotsk Sea, the amplitude reaches a maximum value of 4.2 m as a result of resonance. The natural period of Shelikhova Bay 21 h and its cooscillating amplification factor is about 5 according to Suzuki and Kanari (1986). The amplitude in most of the interior of the bay, then, comes to 5 m with a modeled amplitude of about 1 m at the mouth of the bay. The actual value agrees well with the model value, considering that cooscillation does not take place in Penzhinskaya Bay, the interior part of Shelikhova Bay, in our model. We can also recognize a local minimum near Cape Yelizavety (north of Sakhalin) and relatively higher amplitude along the coasts (to the west of Kamchatka, the east of Sakhalin, and the coast of Okhotsk), which is caused by waves propagating as shelf waves along the coasts as suggested by Odamaki (1994).

The elevation amplitude of the M_2 tide (Fig. 3b) is comparable to that of the K_1 tide and is even larger around the northwestern coast of the Okhotsk Sea. The M_2 tide in the Okhotsk Sea is also largely determined by the incoming tidal wave from the North Pacific (Fig. 4b). After passing through the Kuril Straits, this wave propagates roughly northward as a freely propagating wave, producing two amphidromic points: one in Shelikova Bay and the other near Cape Yelizavety. The M_2 tidal wave partly cooscillates in the northwest and northeast bays, where the elevation amplitude is large (cooscillation in the innermost regions of Shelikova Bay results in a maximum amplitude of 3.6 m.

To study the features of the tidal currents in the Okhotsk Sea, we calculated the ellipse parameters (major and minor semiaxes and angle of inclination) shown in Fig. 6, using the oscillatory component of the calculated velocities. The K_1 tide has the greatest current speed. The currents are strong and their tidal ellipses are circular around topographic feature, such as the Kuril Straits and the Kashebarova Bank. For example, the peak velocity in the northern part of the Kuril Straits attains about 1.6 m s^{-1}, though the maximum value is achieved within the cooscillating Shelikhova Bay. These features are associated considerably with the fact that the period of the K_1 tide (23.93 h) is longer than the inertial period around the Kuril Straits (15.7–17.0 h). Subinertial tidal currents generate subinertial waves trapped at islands and/or submarine banks (e.g., Chapman 1989). The topographically trapped waves are subjected to continuous forcing and are enhanced until damping by friction or viscosity becomes important. The resulting amplification of trapped waves is most effective when the resonance occurs but is significant over a wide range of frequency if the tidal frequency is subinertial (e.g., Haidvogel et al. 1993).

The presence of such topographically trapped waves is clearly seen in the time series of the along-isobath component of velocity around the Kuril Straits (Fig. 7). In particular, clockwise propagation of positive anomalies around Simusir Island, the Urup Strait and Etorof Island, and a bank east of the Kruzenshterna Strait can be easily distinguished. Thus, the K_1 tidal field around

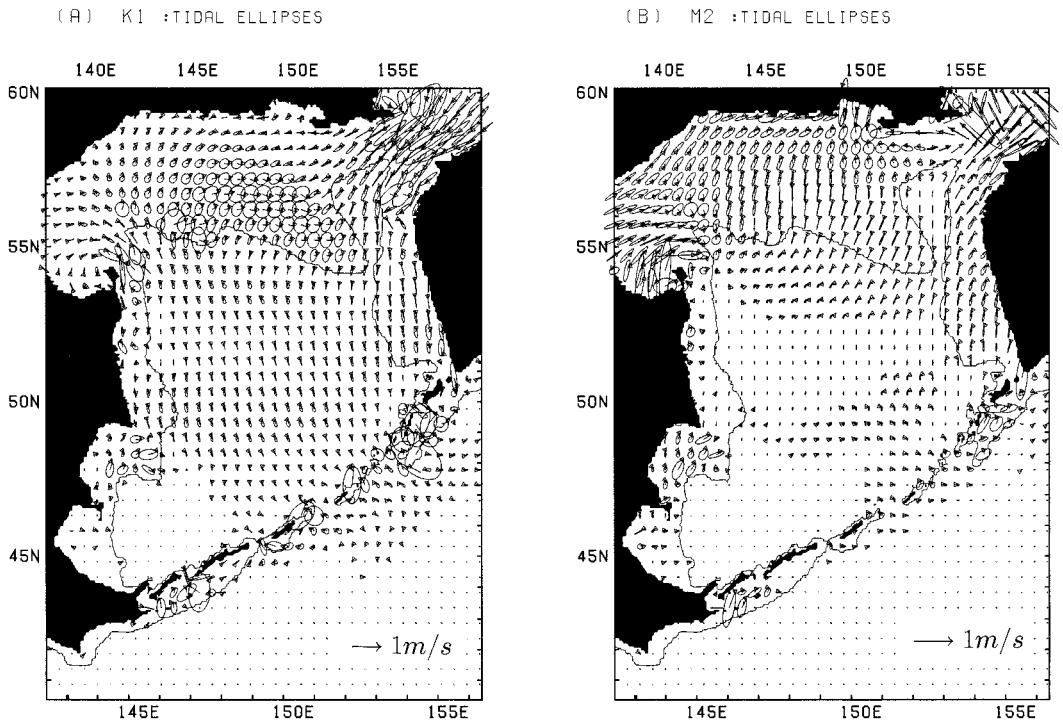

FIG. 6. Calculated tidal ellipses for (a) the K_1 tide and (b) the M_2 tide at every 16 points. The magnitude of velocity is indicated in each figure.

the Kuril Straits is composed of both large-scale K_1 tidal waves coming from the North Pacific and topographically trapped waves. The latter amplifies the currents and makes tidal ellipses circular around the Kuril Straits. Therefore the K_1 tide is expected to cause significant tide-induced mean flow around the straits, which will be discussed in section 4. The along-isobath component of velocities associated with topographic waves is nearly in geostrophic balance since these waves are characteristic of shelf waves and topographic Rossby waves (and Kelvin waves). This may imply that the time-average currents are also roughly geostrophic.

Moderately strong currents near the coasts, where the elevation amplitude is also appreciably larger than that of the surroundings (in Fig. 3a), are thought to be caused by the presence of shelf waves due to the subinertial tidal frequency. Such shelf waves are identified from observations along the Hokkaido coast (Odamaki 1994) and from numerical simulation along the Sakhalin coast (Suzuki and Kanari 1986).

The M_2 tide (Fig. 6b) is substantially smaller in current speed than the K_1 tide, despite the fact that the elevation amplitude is comparable. In contrast to the K_1 tidal currents, the maximum value of the M_2 tidal currents around the Kuril Straits reaches only 0.6 m s^{-1} although the currents are strong within the cooscillating bays in the interior of the Okhotsk Sea. Since the maximum frequencies of barotropic topographic Rossby waves is less than the inertial frequency, topographically trapped waves cannot be generated by superinertial M_2 tides. Indeed, the tidal ellipses are not circular around the Kuril Straits and the Kashebarova Bank. Thus, amplification hardly occurs and the M_2 currents are weak in the Kuril Straits, indicating that the mean currents induced by the M_2 tide are probably not significant.

4. Eulerian mean currents and estimates of tidal exchange through the Kuril Straits

Figure 8 shows the depth-averaged velocity vectors of the Eulerian time-averaged currents over a cycle. For the K_1 tide, significant mean currents near the Kuril Islands can be seen. These currents become especially large in the northern part of the Kuril Straits, where the maximum velocity exceeds 0.7 m s^{-1}, and have in- and outflow components, suggesting that the tidal currents can cause significant long-term exchange through the Kuril Straits. Another interesting feature is the mean current along the coast (with land on the right). These mean currents are almost in geostrophic balance, as expected in section 3. On the contrary, the mean currents around the Kuril Straits induced by the M_2 tide are much smaller than those from the K_1 tide (Fig. 8b).

For closer examination and estimation of the tidal exchange, we calculated the streamfunction of the mean volume transport Ψ, defined as

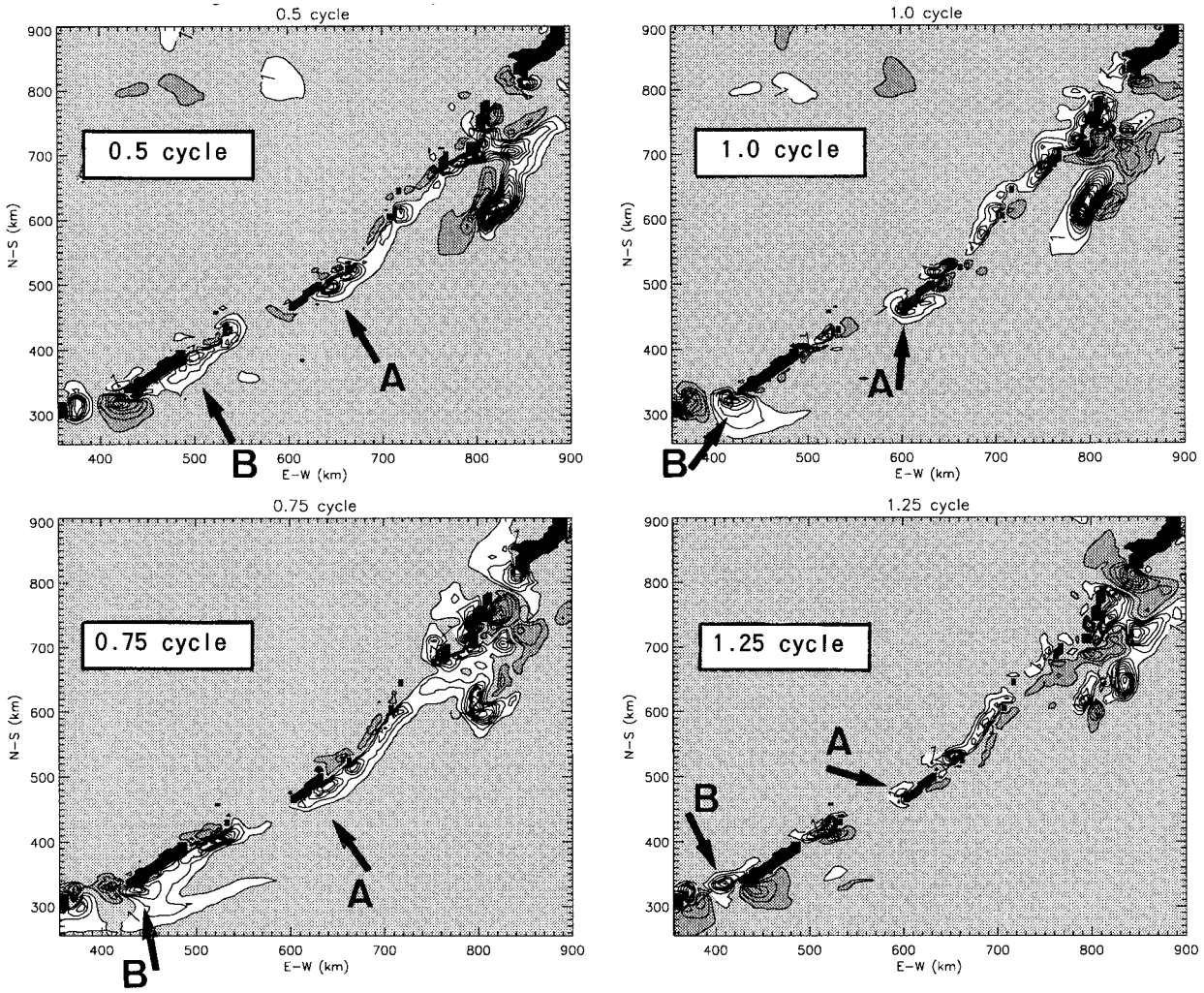

FIG. 7. Temporal change of along-isobath components of velocity around the Kuril Straits with an interval of 0.25 tidal cycle for the K_1 tide. In these panels, clockwise propagation of the disturbance around Simusir Island (the Urup Strait) is indicated by A (B). The contour intervals are 7.5 cm s^{-1}. The current in the non shaded areas (the thicker shaded areas) flows with the shallower water on its right (left), and the current speeds in the thinner shaded areas are less than 7.5 cm s^{-1}.

$$(\overline{u}, \overline{v}) = \left(-\frac{1}{H}\frac{\partial \Psi}{\partial y}, \frac{1}{H}\frac{\partial \Psi}{\partial x}\right), \tag{7}$$

with the zero point taken at the Kamchatka Peninsula. The result for the K_1 tide is shown in Fig. 9. In general, the mean currents are almost parallel to the isobaths and form clockwise mean currents around the islands, leading to bidirectional mean currents in most passages and strong clockwise along-sill (or along-island) mean currents. In particular, a bidirectional flow is pronounced in the Bussol and Kruzenshterna Straits that are relatively wide and deep, while the along-sill currents are strong between the two straits. There is an intense clockwise circulation over the bank to the southeast of Shashikotan Island and an anticlockwise circulation over the Kuril Basin along the isobath.

Taking the bidirectional current structure into account, we estimated the total transport for all the straits with this mean current field. For the K_1 tide (Fig. 10), we can easily see that most of the exchange occurs at Bussol Strait and the northeastern part of the Kuril Straits, and that little transport occurs through the southwestern part where depths are shallow and large islands are present. In terms of magnitude, the net transport of about 5.0 Sv from the Okhotsk Sea to the North Pacific occurs mainly through the Bussol (2.4 Sv), Kruzenshterna (0.8 Sv) and Chetverty (0.8 Sv) Straits. Inflow transport is largest (1.45 Sv) through Bussol Strait followed by 1.2 Sv through Kruzenshterna Strait. Water transported through the straits is carried to the southwest on the Pacific side and to the northeast on the Okhotsk side along the islands by along-sill mean flow. When neglecting the bidirectional flow (i.e., estimating the transport per strait) the total transport comes to 2.2 Sv.

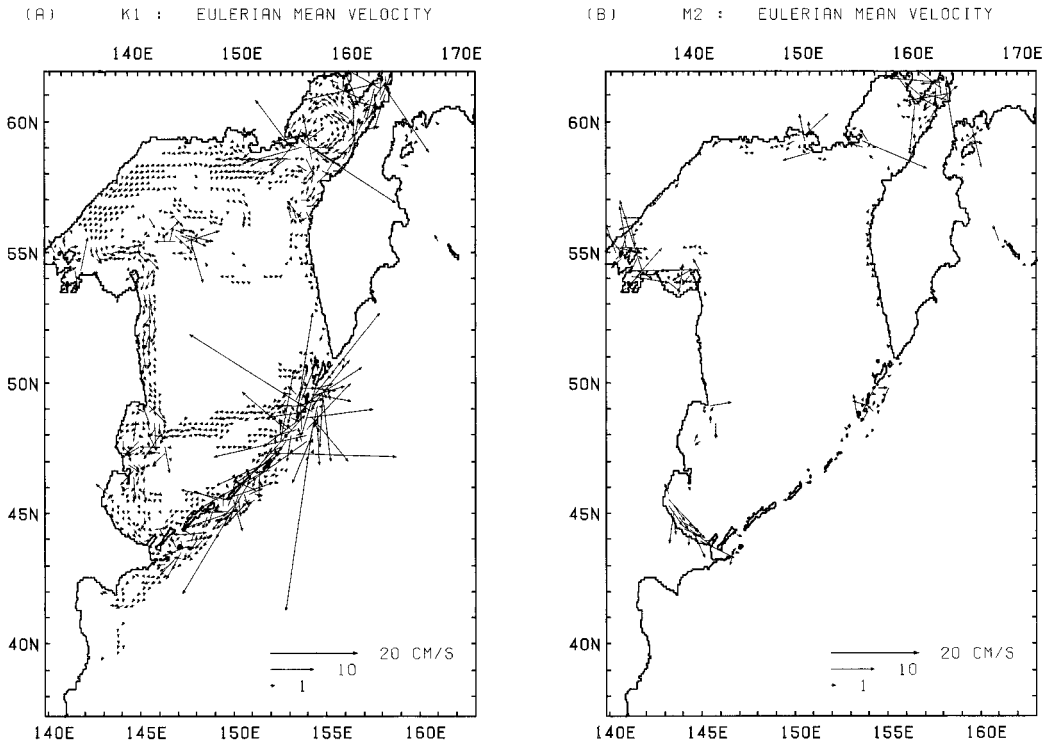

FIG. 8. Eulerian mean currents induced by (a) the K_1 tide and (b) the M_2 tide. The mean currents in regions without arrows are less than 0.5 cm s^{-1}.

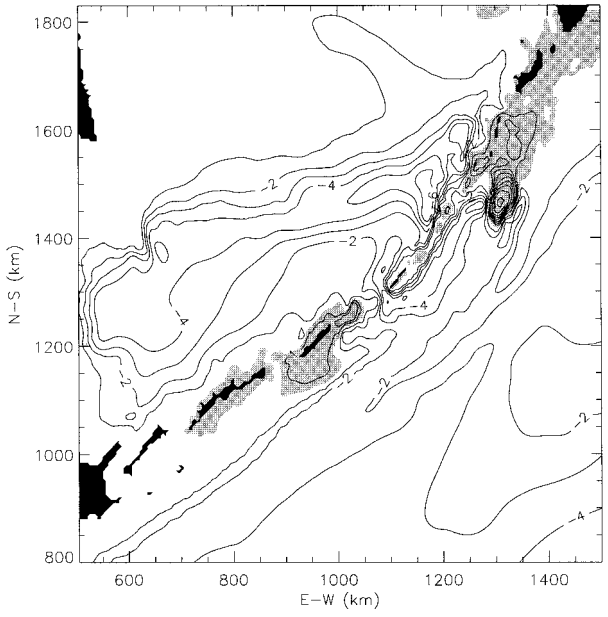

FIG. 9. Mean transport stream function for the K_1 tide, which is set to be zero at the Kamchatka Peninsula. The contour units are 0.4 Sv and values in shaded areas are positive.

This indicates that in order to estimate the total transport observationally, sufficient current meters need to be deployed to detect the bidirectional current structure.

Transport estimates made with the O_1, P_1, M_2, and S_2 tides are 3.5 Sv, 1.0 Sv, 0.3 Sv, and 0.1 Sv, respectively, showing that transport induced by diurnal tides is much greater than that by the semidiurnal tides. With the maximum tidal speeds of 160, 110, 85, 65, and 25 cm s^{-1} for the K_1, O_1, P_1, M_2, and S_2 tides in the Kuril Straits, respectively, the ratios of transports among the diurnal components are almost proportional to their flow speeds. This is also the case for the semidiurnal components but does not hold between diurnal and semidiurnal tides. The transport by diurnal tides is considerably larger than that expected from the ratio of diurnal to semidiurnal current speeds. For example, the K_1 transport is about 17 times as large as the M_2 transport whereas the K_1 flow speed is only about 2.5 times that of M_2. Thus, whether tides are subinertial or not is anticipated to have a large effect on the difference in mean transport between the diurnal and semidiurnal tides.

5. Formation mechanism of bidirectional mean currents in the Kuril Straits

a. Vorticity analysis

In order to investigate the formation mechanism of the mean flow, we first make an analysis of vorticity

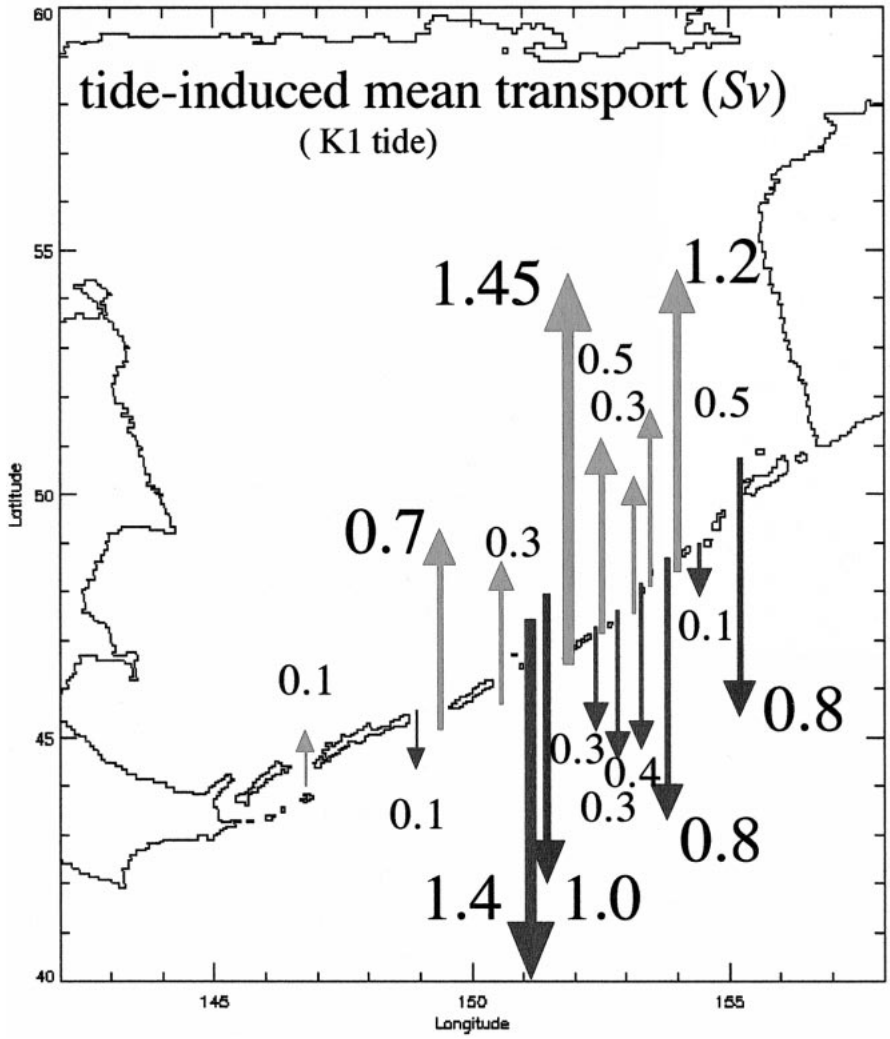

FIG. 10. The estimate of the mean transport through the Kuril Straits induced by the K_1 tide. Upward and downward arrows represent inflow and outflow, respectively.

focusing on the K_1 case, because the K_1 component dominates the mean transport and because the formation mechanism may be helpful in clarifying the cause for the difference in mean transport between the diurnal and semidiurnal tides. The vertical component of vorticity ω is defined as the depth-averaged relative vorticity

$$\omega = \frac{\partial v}{\partial x} - \frac{\partial u}{\partial y}. \tag{8}$$

Figure 11 shows the Eulerian mean relative vorticity over a cycle around the Kuril Straits. According to previous studies of tidal rectification (e.g., Robinson 1981), the mean vorticity generally acquires negative values on the sill top and positive values at the base of the sill, which, in turn, produce a clockwise mean current along the sill since mean currents are almost zero far away from the sill. Such a pattern is clearly seen in shallow straits (200~600 m depth). A close look at Fig. 11 shows that as the sill gets higher in the vicinity of the islands, the magnitude of the negative mean vorticity on the top of the sill becomes larger. Supposing mass conservation of the along-sill mean currents, such vorticity changes in shallow straits lead to clockwise mean circulation on island scales, thus creating bidirectional mean currents in shallow straits as is shown schematically in Fig. 12a.

In deep straits, on the other hand, the mean vorticity distribution on the sill top has positive values near the islands (except for thin viscous boundary layers closer to islands). This vorticity pattern differs greatly from that in shallow straits in spite of the presence of similar bidirectional currents (Fig. 11). To investigate this problem, we direct our attention to Bussol Strait, where the

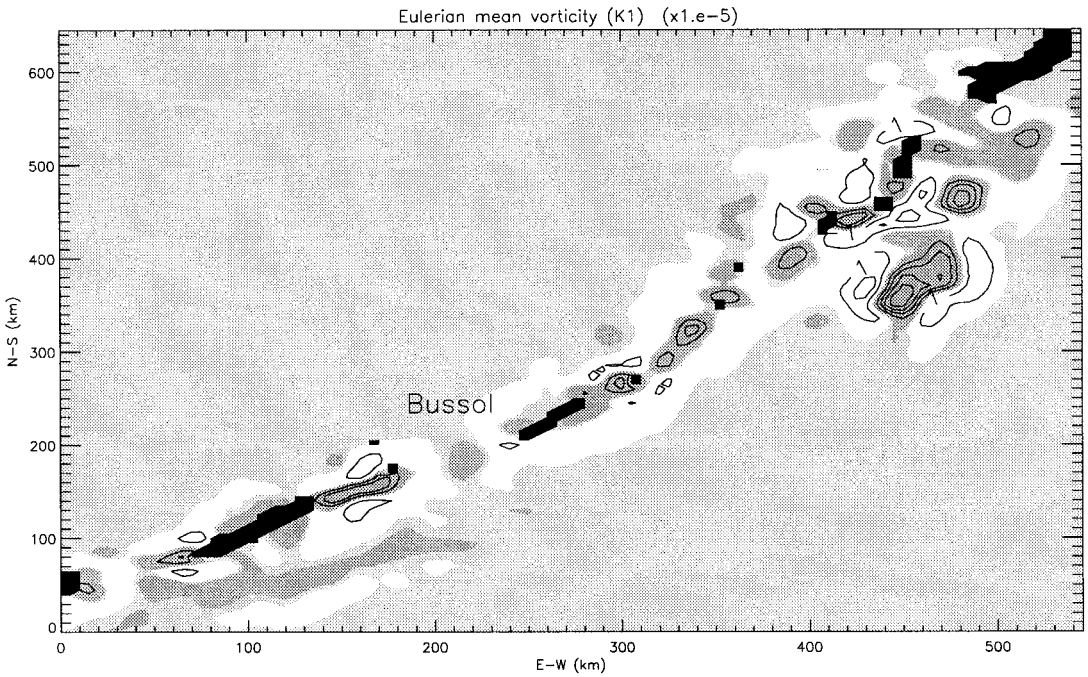

FIG. 11. The Eulerian mean relative vorticity over one cycle around the Kuril Straits for the K_1 tide. The contour interval is 1×10^{-5} s^{-1}. Values in nonshaded areas and the thicker shaded areas are positive and negative, respectively, and the absolute values in the thinner shaded areas are less than 1×10^{-6} s^{-1}.

sill is very deep, bidirectional currents are dominant, and hence most of the outflow from the Okhotsk Sea occurs. The vorticity distributions around the strait are as follows. (i) A positive mean vorticity is located in the western part of Bussol Strait (near the shallow Urup Strait). (ii) In the central part of Bussol Strait, a negative mean vorticity is present over the deep sill. (In contrast to shallow sills, the positive mean vorticity at the foot of the sill is too small to be distinguished and has little influence.) (iii) A positive mean vorticity is located in the eastern part of Bussol Strait. The mean vorticity distribution (i) produces strong clockwise mean currents, flowing out with a transport of 1.4 Sv through the western part of Bussol Strait to the southwest along the Kuril Island Chain. The distributions (ii) and (iii) merge to produce a mean outflow of 1.0 Sv to the southeast from the middle of Bussol Strait [intermediate to the distributions (ii) and (iii)]. The distribution (iii) produces a strong mean inflow of 1.45 Sv along Simusir Island (east of Bussol Strait). It is worth mentioning that the mean vorticity values in Bussol Strait are so small that a slow mean flow is produced, though the deep strait (over 2000 m) makes the overall mean transport significant. In this way, the mean vorticity produces bidirectional mean currents and a slow centered-outflow in Bussol Strait, as is shown schematically in Fig. 12b.

To examine the cause for the different vorticity distribution between deep and shallow straits, we first diagnose the temporal evolution of the vorticity balance in a similar way to Ridderinkhof (1989), because our interest is in the generation mechanism of bidirectional current structures in the Kuril Straits. Taking the curl of the momentum equation (1) yields the vorticity equation as

$$\frac{D\omega}{Dt} = \underbrace{-f\nabla\cdot\mathbf{u}}_{(a)} \underbrace{-\omega\nabla\cdot\mathbf{u}}_{(b)} + \underbrace{\kappa\mathbf{u}\times\frac{\nabla|\mathbf{u}|}{H+\eta} + \kappa\mathbf{u}\times|\mathbf{u}|\nabla\left(\frac{1}{H+\eta}\right)}_{(c)} \underbrace{-\frac{\kappa|\mathbf{u}|}{H+\eta}\omega}_{(d)} + \underbrace{A_H\nabla^2\omega}_{(e)}, \quad (9)$$

where D/Dt represents the time variation in the Lagrangian frame and the β term and the terms arising from the spatial variation of horizontal eddy viscosity are neglected because of their smallness. The sum of terms on the rhs of Eq. (9) represents the mechanisms generating and damping vorticity. Terms (a) and (b) generate vorticity by stretching or squeezing of a water column through the conservation of potential vorticity. For term (a), the vorticity generated by stretching (squeezing) acquires positive (negative) values. Term (c) represents vorticity generation due to velocity shear (for a quadratic friction law) and the horizontal gradient of water depth transverse to the direction of the tidal

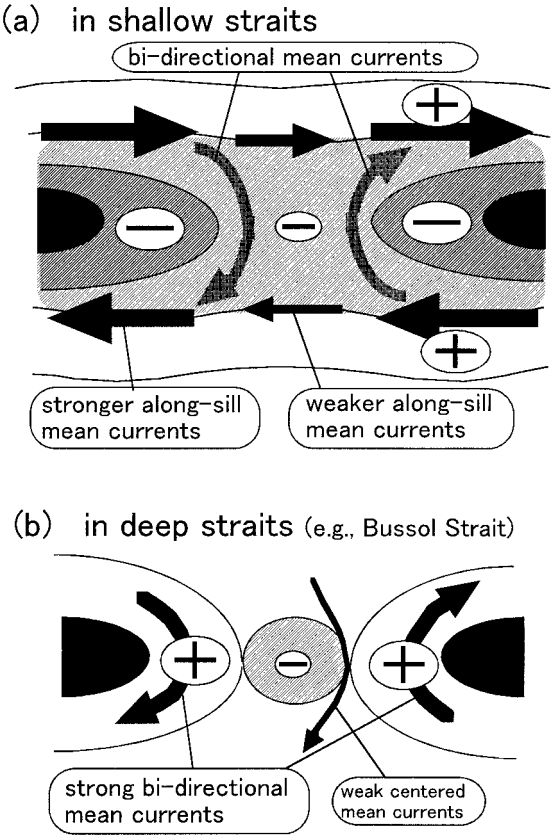

FIG. 12. Schematic illustrations of mean currents associated with the mean vorticity distribution in (a) shallow straits (200~600-m depth) and (b) deep straits (the case of the Bussol Strait).

flow. Term (d) represents the damping part of bottom friction. Term (e) causes a damping of vorticity through the horizontal eddy viscosity.

Though the vorticity balance is examined during a tidal cycle, we show the spatial distributions of each term on the rhs of Eq. (9) only when the outflow speed is a maximum in Bussol Strait (Fig. 13). The features described below are essentially similar for the other tidal phases. In general, as in the previous studies, the stretching/squeezing term (a) from the Coriolis effect is most effective in vorticity generation while the other stretching/squeezing term (b) is less so, with the exception that term (b) is quite significant in regions of strong relative vorticity such as over the bank to the southeast of Shashikotan Island. The vorticity generation due to bottom friction is much smaller than that due to these terms except in spatially small shallow regions (depth less than 100 m) such as in the vicinity of Onnekotan Island, where water exchange between the Okhotsk Sea and the North Pacific is not significant. The damping of vorticity is caused primarily by bottom friction, and the effect of horizontal eddy viscosity is negligible when compared to that of bottom friction. Thus, the vorticity sources for generating the bidirectional current structure are thought to be similar in both shallow and deep straits, despite that their vorticity distributions differ. This implies the presence of a different physical process from the previous tidal rectification theory (e.g., Robinson 1981) for the formation of the mean circulation in deep straits. Previously, vorticity (nonaveraged) was generated by tidal currents over variable topography and redistributed by advection, eventually forming a time-averaged vorticity distribution with positive (negative) located on the shallower (deeper) side when stretching/squeezing terms are dominant in the vorticity equation. This is certainly the case for the present shallow straits but is not the case for the deep straits. The most likely candidate for generating the mean circulation in deep straits is the effect of topographically trapped waves, discussed below.

b. Generation mechanism of bidirectional mean currents in deep straits

To identify a possible role for topographically trapped waves (TTW) in the vorticity balance, we first look at the temporal change of vorticity around the deep Bussol Strait (Fig. 14). On the northern side of the shallow Urup Strait (west of Bussol Strait), a significant portion of positive vorticity (nonshaded in Fig. 14) generated at flood tide (after 0 h; Fig. 14a) propagates clockwise and enters the deep Bussol Strait (Figs. 14b–c), while negative vorticity (thicker) at ebb tide (Fig. 14e) scarcely moves (Figs. 14f–h). Similar propagation is seen to the north of Simusir Island (east of Bussol Strait). From these results, one may speculate that the difference in propagation of positive and negative vorticity anomalies may create positive mean vorticity in the southwestern and northeastern parts of Bussol Strait, which is capable of producing bidirectional mean currents as illustrated in Fig. 12b.

In previous studies on subinertial tidal currents (e.g., Chapman 1981; Kowalik and Proshutinsky 1995), these vorticity anomalies propagating along isobaths are attributed to TTWs. In fact, the frequency of these anomalies is estimated as 0.5×10^{-4} (rad s^{-1}), using a linear dispersion relation of TTW on a constant slope α with mean depth H,

$$\sigma = -f\frac{\alpha}{H}k\left(k^2 + l^2 + \frac{1}{4}\frac{\alpha^2}{H^2} + \frac{f^2}{gH}\right)^{-1}, \quad (10)$$

where σ is the frequency, k is the wavenumber in the along-isobath direction and l in the across-isobath direction. These values are taken from the figure ($H \sim$ 700 m, $\alpha \sim 0.1$, $2\pi/k \sim 40$ km, $2\pi/l \sim 40$ km). The estimated frequency roughly agrees with the K_1 frequency (0.7×10^{-4} rad s^{-1}), implying that these anomalies are TTWs generated by the incoming K_1 tidal wave. Although most previous studies on tidal exchange have paid little attention to the role played by TTWs, the above facts strongly suggest that the propagation of vor-

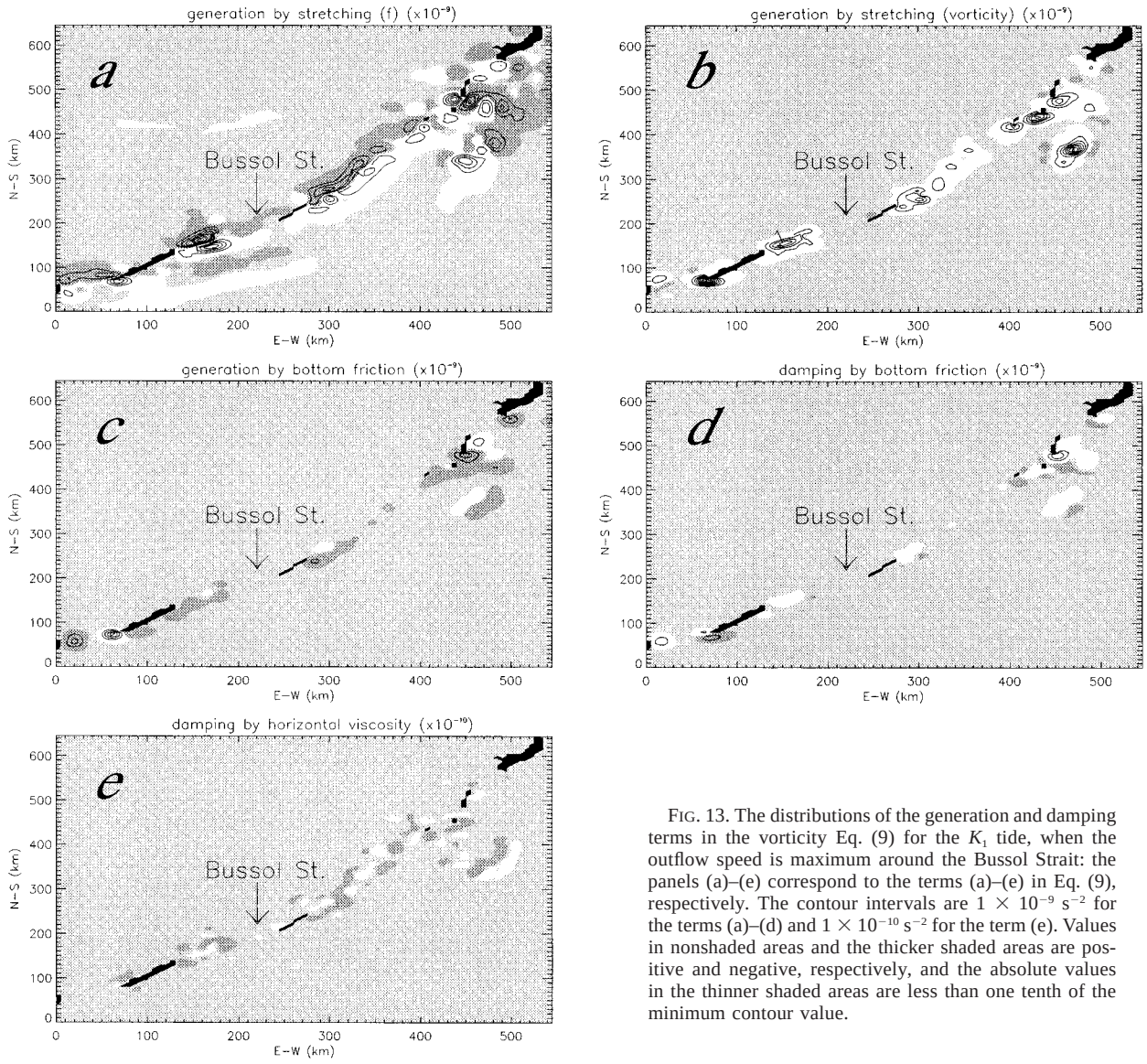

FIG. 13. The distributions of the generation and damping terms in the vorticity Eq. (9) for the K_1 tide, when the outflow speed is maximum around the Bussol Strait: the panels (a)–(e) correspond to the terms (a)–(e) in Eq. (9), respectively. The contour intervals are 1×10^{-9} s^{-2} for the terms (a)–(d) and 1×10^{-10} s^{-2} for the term (e). Values in nonshaded areas and the thicker shaded areas are positive and negative, respectively, and the absolute values in the thinner shaded areas are less than one tenth of the minimum contour value.

ticity anomaly as TTWs may be effective in the vorticity balance around the Kuril Islands for subinertial tides such as the K_1 tide. Focusing on this point, we investigate the generation mechanism of mean vorticity in the Kuril Straits.

We begin with the following vorticity equation,

$$\frac{\partial \omega}{\partial t} + \mathbf{u} \cdot \nabla \omega = -f \nabla \cdot \mathbf{u} + \text{damping}, \qquad (11)$$

where only the dominant vorticity-generation term (a) in Eq. (9) at the Kurils is taken into account for simplicity. Note that, though the β term permits the presence of barotropic Rossby waves, this term can be neglected in comparison with topographic variation in the Kuril Straits. This is because the topography influence dominates β when $|\nabla H|/H > \beta/f_0$ (e.g., LeBlond and Mysak 1978), which is roughly estimated as the inequality $10^{-7} \gg 10^{-9}$.

Since the propagation of TTWs such as topographic Rossby waves relates to vorticity change in space and time, we separate the velocity field according to Holton (1979) as follows. The Helmholtz theorem states that any velocity field $\mathbf{V}$ can be divided into a nondivergent part $\mathbf{V}^{\psi}$ plus an irrotational part $\mathbf{V}^{\text{irr}}$ such that

$$\mathbf{V} = \mathbf{V}^{\psi} + \mathbf{V}^{\text{irr}}, \qquad (12)$$

where $\nabla \cdot \mathbf{V}^{\psi} = 0$ and $\nabla \times \mathbf{V}^{\text{irr}} = 0$. If the velocity field is two dimensional and is denoted by $\mathbf{V} = (U, V)$, the nondivergent part can be expressed in terms of the streamfunction ψ defined by

$$(U^{\psi}, V^{\psi}) = \left(-\frac{\partial \psi}{\partial y}, \frac{\partial \psi}{\partial x}\right). \quad (13)$$

While previous studies focus mainly on the advection of vorticity in the across-isobath direction, TTWs propagate along the isobaths. Taking this fact into account, we take the coordinate x (y) to represent the northeast (northwest) direction, which is almost along (across) the sills in the Kuril Island Chain. Accordingly, $H_x \ll H_y$ and the component U basically represents the along-isobath velocity component and V the across-isobath component. The across-isobath velocity V generates a net across-isobath advection of vorticity through the well-known mechanism of tidal rectification over variable topography, thus producing mean along-isobath currents (e.g., Robinson 1981). The vorticity can also be advected in the along-isobath direction by the velocity component U.

The stretching/squeezing of water columns by the motion of the free surface can be neglected when $f^2L^2/gH \ll 1$, where L is the horizontal length scale taken as the lesser of the topographic length scale or wavelength (e.g., LeBlond and Mysak 1978). In the K_1 case, L is less than several tens of kilometers, giving a divergence parameter f^2L^2/gH of the order of 10^{-2}. Thus a rigid lid approximation is a reasonable simplification. Hence, the continuity equation (2) yields

$$H\nabla \cdot \mathbf{u} = -\nabla H \cdot \mathbf{u}. \quad (14)$$

Using the notation for $\mathbf{V}$ given in Eq. (12), the rhs of Eq. (14) is written as

$$-\nabla H \cdot \mathbf{V} = -\nabla H \cdot (\mathbf{V}^{\psi} + \mathbf{V}^{\mathrm{irr}}). \quad (15)$$

Note that under the present approximation, $\mathbf{V}^{\mathrm{irr}}$ represents the divergent component when neglecting the contribution of sea surface elevation to the volume transport.

Substitution of Eqs. (12)–(15) into Eq. (11) yields

$$\left(\frac{\partial}{\partial t} + \mathbf{V} \cdot \nabla\right)\omega - \frac{f}{H}\left(-H_x\frac{\partial \psi}{\partial y} + H_y\frac{\partial \psi}{\partial x}\right) = \frac{f}{H}\nabla H \cdot \mathbf{V}^{\mathrm{irr}} + \text{damping}. \quad (16)$$

To examine the vorticity balance in the vicinity of the Kuril Straits in detail, we look at the temporal changes of both velocity and vorticity in the shallow Urup Strait during one cycle as an example (Fig. 15). As the northwestward K_1 current flowing into the Okhotsk Sea runs over the sill, it is clear that a strong northeastward current appears over the sill after 0.25 cycle (Fig. 15b) due to the occurrence of the along-isobath current arising from topographic rectification of the K_1 current over the sill. Another conspicuous feature in Fig. 15 is the generation of significant vorticity anomalies in both positive and negative senses on the down- and upstream sides of the sill, respectively. The vorticity anomalies largely propagate along the isobaths [for example, northeastward (southwestward) propagation of the positive (negative) vorticity anomaly in Figs. 15a,b]. This propagation could be associated with TTWs because the propagation of TTWs is caused by the difference in the magnitude of vorticity in the along-isobath direction (e.g., Longuet-Higgins 1965) and swifter currents within the strait do, in fact, produce stronger vorticity than in other regions. In the latter half cycle, almost all of these features can be seen but their phase is reversed. However, the propagation of vorticity anomalies is in the same direction as in the previous half cycle.

Considering that an incident K_1 wave has very small vorticity in deep regions (one or two orders of magnitude less than in the straits; Figs. 14 and 15) and that vorticity change is caused almost solely by the change of f/H, the component $\mathbf{V}^{\psi}$ in a slope region may be dominated by the contribution from the vorticity generated by the stretching/squeezing effect. To conveniently identify the role of TTWs in the vorticity balance around the Kuril Islands, we define the velocity component associated with TTWs ($\mathbf{V}^{\psi}_{\mathrm{TTW}}$) as that representing the propagation of the vorticity anomalies. The relevance of this will be discussed later. The remainder ($\mathbf{V}^{\psi}_{\mathrm{rec}}$) is hereafter called the rectified temporal current in parallel with previous tidal rectification studies (e.g., Robinson 1981), although it is in general difficult to separate the velocity components associated with TTWs from the rectified temporal currents because both are topographically produced.

Taking the above facts into account, we therefore separate the nondivergent velocity component $\mathbf{V}^{\psi}$ as

$$\mathbf{V}^{\psi} = \mathbf{V}^{\psi}_{\mathrm{TTW}} + \mathbf{V}^{\psi}_{\mathrm{rec}}. \quad (17)$$

These are expressed in terms of the streamfunctions as

$$\mathbf{V}^{\psi}_{\mathrm{TTW}} = \left(-\frac{\partial \psi_{\mathrm{TTW}}}{\partial y}, \frac{\partial \psi_{\mathrm{TTW}}}{\partial x}\right),$$

$$\mathbf{V}^{\psi}_{\mathrm{rec}} = \left(-\frac{\partial \psi_{\mathrm{rec}}}{\partial y}, \frac{\partial \psi_{\mathrm{rec}}}{\partial x}\right), \quad (18)$$

where ψ_{TTW} and ψ_{rec} are the streamfunctions for the TTWs and the rectified current.

We assume that the wave solution for the streamfunction ψ_{TTW} associated with TTWs is given as

$$\psi_{\mathrm{TTW}} = \hat{\psi}_{\mathrm{TTW}} e^{i(kx+ly-\sigma t)}, \quad (19)$$

→

FIG. 14. The time series of vorticity anomalies around Bussol Strait after (a) 0.0, (b) 0.125, (c) 0.25, (d) 0.375, (e) 0.5, (f) 0.625, (g) 0.75, and (h) 0.875 cycle. The contour interval is 1×10^{-5} s^{-1}. Values in non shaded areas and the thicker shaded areas are positive and negative, respectively, and the absolute values in the thinner shaded areas are less than 0.5×10^{-5} s^{-1}.

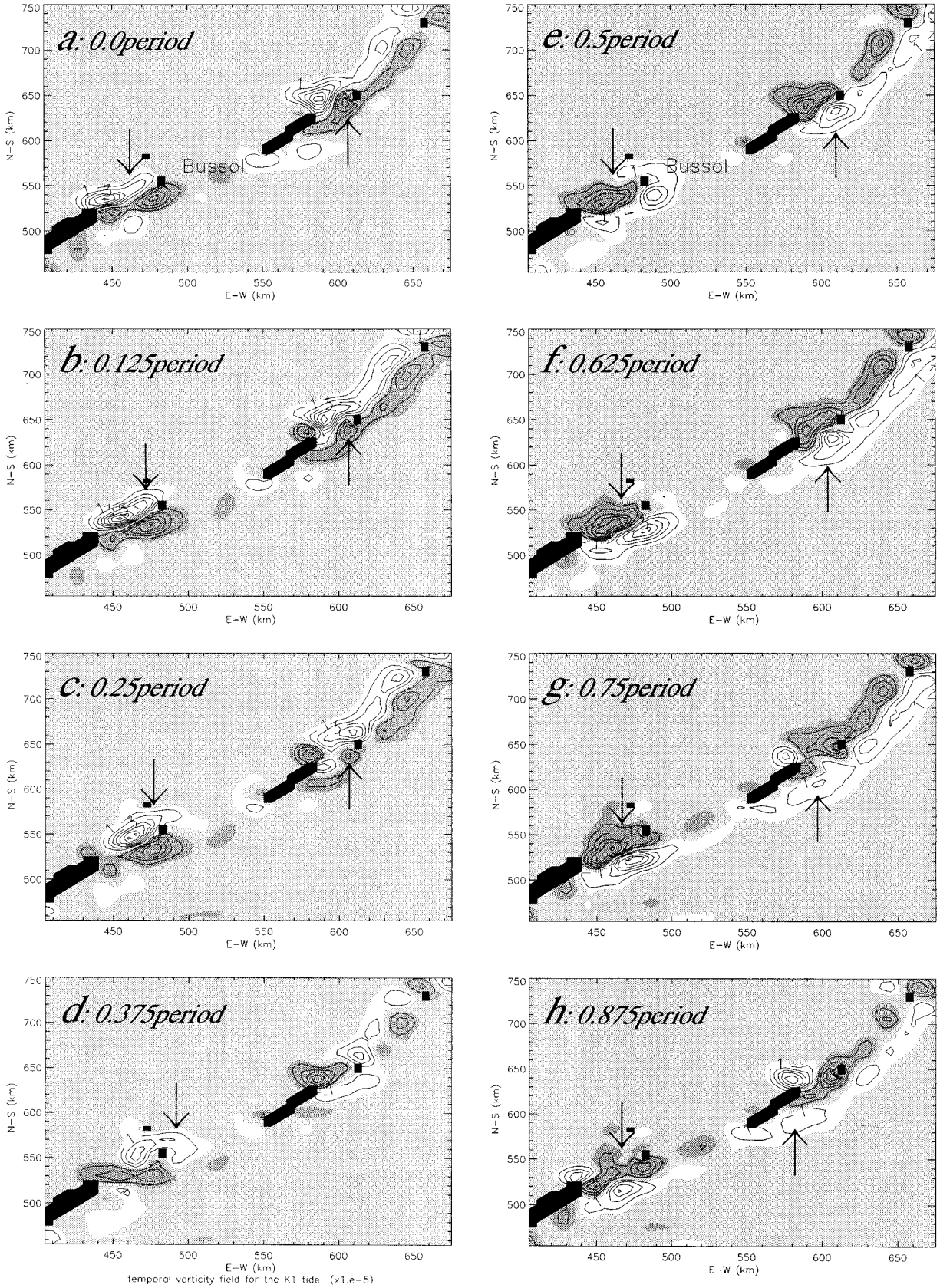
a: 0.0period
b: 0.125period
c: 0.25period
d: 0.375period
e: 0.5period
f: 0.625period
g: 0.75period
h: 0.875period
Bussol
N-S (km)
E-W (km)
750
700
650
600
550
500
450
500
550
600
650
temporal vorticity field for the K1 tide (x1.e-5)

where k and l are the wavenumbers in the x and y directions, respectively. Using Eqs. (17)–(19), the second term on the lhs of Eq. (16) becomes

$$-\frac{f}{H}(-H_x il + H_y ik)\psi_{\mathrm{TTW}} - \frac{f}{H}\nabla H \cdot (\mathbf{V}^{\psi} - \mathbf{V}^{\psi}_{\mathrm{TTW}})$$

$$= (c_x ik + c_y il)(-k^2 - l^2)\psi_{\mathrm{TTW}} - \frac{f}{H}\nabla H \cdot \mathbf{V}^{\psi}_{\mathrm{rec}}$$

$$= \mathbf{c} \cdot \nabla \omega_{\mathrm{wave}} - \frac{f}{H}\nabla H \cdot \mathbf{V}^{\psi}_{\mathrm{rec}}. \quad (20)$$

Here, ω_{wave} is the vorticity component associated with ψ_{TTW} such that

$$\nabla \times \mathbf{V}^{\psi}_{\mathrm{TTW}} = \nabla^2 \psi_{\mathrm{TTW}} = \omega_{\mathrm{wave}}. \quad (21)$$

The quantity $\mathbf{c} = (c_x, c_y)$ in Eq. (20) represents the phase speed of the vorticity anomalies and is given by

$$c_x = \frac{H_y}{k^2 + l^2}\frac{f}{H}, \qquad c_y = -\frac{H_x}{k^2 + l^2}\frac{f}{H}. \quad (22)$$

Interestingly, this is the same form as the phase velocity of a nondivergent linear topographic Rossby wave (e.g., Cushman-Roisin 1994). Since $H_x \ll H_y$, the propagation of the vorticity ω_{wave} is dominated by the component c_x. Substitution of Eq. (20) into Eq. (16) yields

$$\left(\frac{\partial}{\partial t} + (\mathbf{V} + \mathbf{c}) \cdot \nabla\right)\omega_{\mathrm{wave}} + \left(\frac{\partial}{\partial t} + \mathbf{V} \cdot \nabla\right)(\omega - \omega_{\mathrm{wave}})$$

$$= \frac{f}{H}\nabla H \cdot (\mathbf{V}^{\mathrm{irr}} + \mathbf{V}^{\psi}_{\mathrm{rec}}) + \text{damping}. \quad (23)$$

Equation (23) shows that the interaction between the net across-sill (across-isobath) current and the topography

$$\frac{f}{H}\nabla H \cdot (\mathbf{V}^{\mathrm{irr}} + \mathbf{V}^{\psi}_{\mathrm{rec}})$$

generates two vorticity components that are governed by different dynamics. Note that as in previous studies, $\mathbf{V}^{\psi}_{\mathrm{rec}}$ is dominated by the along-isobath component and, hence, the effect of the current associated with the K_1 tidal waves ($\sim\mathbf{V}^{\mathrm{irr}}$) coming from the North Pacific dominates the vorticity generation in the Kuril Straits. The vorticity component ($\omega - \omega_{\mathrm{wave}}$) is transported only by advection and causes the well-known process of tidal rectification (e.g., Chen and Beardsley 1995). In contrast, the transport of the vorticity anomaly ω_{wave} is driven not only through advection by the currents (U, V) but also by the propagation of TTWs with phase speed **c**. This means that there are additional vorticity changes caused by the propagation of TTWs at all locations along the wave paths. Accordingly, TTWs are able to affect the mean vorticity field at locations (e.g., the deep Bussol Strait) well away from the generation region (e.g., the shallow Urup Strait). This effect has important implications but is absent unless both subinertial tides and the variation in the along-isobath direction are considered.

To easily assess whether or not the treatment of TTWs in this study [Eqs. (17)–(19)] is reasonable, we make a comparison between the intrinsic phase speed c_x estimated from Eq. (22) and that appearing in the model results, for example, around Urup Strait as shown in Fig. 15. Equation (22) for the intrinsic phase speed c_x of ω_{wave} in the along-isobath direction yields approximately ± 0.3 m s^{-1} on the northern (southern) side of the sill using the values estimated earlier. On the other hand, in Figs. 15a,b, the apparent speed of the positive (negative) vorticity anomaly corresponding to **A** (**B**) in the along-sill direction is estimated to be about $+1.0$ m s^{-1} (-0.1 m s^{-1}). According to Eq. (23), the intrinsic phase speed c_x of these anomalies is given by subtracting the along-isobath current speed U from the apparent speeds of the vorticity anomalies. Since the corresponding speed U calculated in the model is about $+0.6$ m s^{-1} ($+0.2$ m s^{-1}) for the positive (negative) anomaly, so the intrinsic phase speed c_x of the modeled positive (negative) anomaly seen in Fig. 15 is estimated approximately as $+0.4$ m s^{-1} (-0.3 m s^{-1}), in good agreement (approximately 80%) with the value of c_x of the vorticity anomaly corresponding to ω_{wave} from Eq. (22). Note that both anomalies move with the shallower side on the right in a similar sense to TTWs. This provides some support for the treatment of TTWs in this study.

Based on the above consideration, the formation of the bidirectional mean current in deep straits such as Bussol Strait can be interpreted as follows. In the Northern Hemisphere, the intrinsic phase velocity **c** of TTWs is in the along-isobath direction with shallower regions on the right. When the K_1 tidal current moving toward the Okhotsk Sea flows over a sill such as that in the shallow Urup Strait adjacent to the deep Bussol Strait, the along-sill (along-isobath) current U is generated on the sill slope and flows like a rectified temporal current with a positive (negative) value of topographically generated vorticity to the north (south), as seen in Fig. 15b. At this moment, on the positive vorticity side to the north of the sill top, the along-sill current (U) is in the same direction as the intrinsic phase velocity (c_x) of the TTWs with positive vorticity anomaly, as is shown schematically in Fig. 16b. In contrast, on the negative vorticity side to the south of the sill top, the along-sill current (U) is in the opposite direction to the propagation of TTWs of negative vorticity anomaly. When the K_1 tidal current reverses, a similar situation occurs but the positive (negative) vorticity side is to the south (north) of the sill. Consequently, the TTWs with positive vorticity anomaly appearing on the downstream side of the sill move faster than those with negative vorticity on the upstream side of the sill due to the difference in the direction between the phase velocity (c_x) and the along-sill current (U) during the ebb and flood tides as seen in Fig. 15. This means, in a sense, that the magnitude of the positive vorticity flux created by TTWs in

the along-isobath direction is larger than that of the negative vorticity flux over a tidal cycle, and eventually leads to the presence of a net flux of positive vorticity in a clockwise sense around the islands as schematically illustrated in Fig. 16c.

In shallow straits, since TTWs hardly cross the shallow sills, the above process has little effect on the formation of mean vorticity. In contrast, in deep and wide straits such as the Bussol and Kruzenshterna Straits, mean vorticity generation through the classical tidal rectification process is small but the TTWs coming from the adjacent shallow straits such as Urup Strait can cross the deep sills, thus producing positive mean vorticity. This leads to the formation of a bidirectional mean current structure around both ends of the deep sills. In addition, weak negative mean vorticity generated by large-scale tidal currents in the central part of the straits remains unaffected by TTWs. These processes may produce the mean vorticity distribution illustrated in Fig. 12b.

Rough estimates of the transport associated with the TTWs for the K_1 tide is about 50% of the total transport, assuming that the transport by the bidirectional currents in the Bussol (the outflow from the central part is excluded) and Kruzenshterna Straits are due to TTWs. Thus, TTWs play an important role in producing effective water exchange through the Kuril Straits in the model, by generating strong bidirectional mean currents in deep and wide straits. However, this mechanism has little effect on tidal exchange for the case of superinertial tides (e.g., the M_2 tide) because they are inefficient generators of TTWs as seen in section 3. This is a possible explanation for the fact that subinertial diurnal tides cause more efficient water exchange through the Kuril Straits than superinertial semidiurnal tides, as estimated in section 4.

6. Discussion

Although we used a quadratic friction form in this study, a different scheme for bottom friction may lead to different results in coastal embayments (shallower than some tens of meters) according to past studies. However, bottom friction is not strong enough to change the calculated current field in the Kuril Straits qualitatively because most straits are deeper than several hundred meters. In fact, the term balance of the vorticity equation (Fig. 13) shows that the bottom friction terms are more than one order of magnitude less than the dominant stretching/squeezing terms in the Kuril Straits, except in very shallow and narrow regions (some tens of meters deep). Thus, the essential results obtained here are largely valid, with the proviso that the strength of mean currents is somewhat changeable for the choice of the friction law. For example, Huthnance (1981) indicated by analytical study that the magnitude of a mean current produced by the quadratic friction form is 2/3 times that by linear friction and the current structures are qualitatively the same. However, when undertaking the modeling problem in shallow embayments in coastal region, some improvements to this model will be necessary.

We performed another experiment for the K_1 tide in which grid sizes were reduced to 2.5 km $\times$ 2.5 km since the resolution of topographically trapped waves (a wavelength or about 40 km) is not sufficient. The result shows better agreement with observations of elevation and the rms error reduces by 1 cm. The qualitative features of the calculated mean current field is common in both cases although the amount of water exchange through the straits becomes 9.5 Sv (Fig. 17). Despite the substantial increase in mean transport, the increase of maximum current and mean current speeds in the Kuril Straits are about 20% (1.6 to 1.9 m s^{-1}) and 30% (0.7 to 0.9 m s^{-1}), respectively. The current structure of a topographically trapped wave (e.g., in Urup Strait) is reproduced more clearly (not shown). These are probably due to the better resolution of current structure, vorticity generation in a slope region and thus topographically trapped waves. The better resolution may result in greater water exchange.

In section 5b, we neglected the ω term (b) (i.e., $-\omega\nabla \cdot \mathbf{u}$) in the formulation of the generation of bidirectional mean currents in deep straits. Here, we briefly discuss the effect of this on the generation of bidirectional mean currents in deep straits based on Eq. (23), which is the final formula for the analysis. When term (b) is taken into consideration, the intrinsic phase velocity $\mathbf{c}$ and the forcing term on the rhs of Eq. (23) are altered through the change of f to $f + \omega$. As for the phase velocity, Eq. (22) implies that the along-isobath phase speed (c_x) of TTWs on the positive (negative) vorticity side increases (decreases) in the northern hemisphere. For example, when the magnitude of ω is assumed to be 0.2×10^{-4} (a typical value in the present shallow straits), the speed increases (decreases) by about 20% on the positive (negative) vorticity side. This acts to enhance the net positive vorticity flux from shallow straits to deep straits, which is described in section 5b. Similarly, the change in the forcing term strengthens (weakens) the generation of positive (negative) vorticity. Thus, the net effect becomes significant as relative vorticity ω increases, modifying the net positive vorticity flux to deep straits from that expected from Eq. (23). However, once relative vorticity is transported away from shallow straits into deeper regions by TTWs, the subsequent transport and the resulting mean vorticity formation could be qualitatively similar to that explained in section 5b because relative vorticity in the deep regions is expected to be very small.

We investigated the basic features and the generation mechanism of mean transport for each component. However, it is desirable to run the model with several tidal components simultaneously in order to make an actual quantitative estimate of tidal exchange. According to Kowalik and Polyakov (1998), the K_1 and O_1

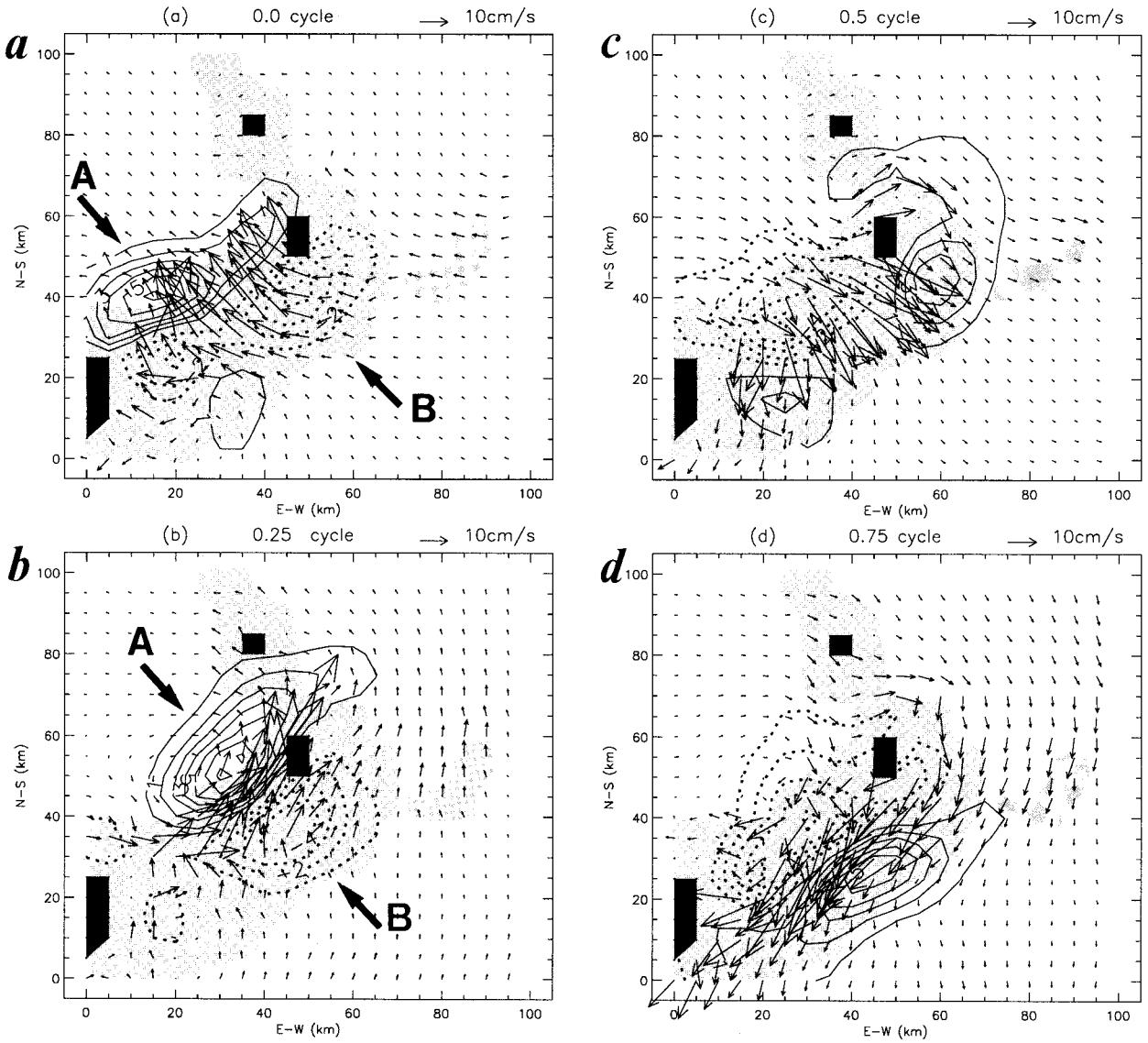

FIG. 15. Isolines of vorticity and the K_1 tidal current vectors around the shallow Urup Strait after (a) 0.0, (b) 0.25, (c) 0.5, and (d) 0.75 cycle. The contour interval is 1×10^{-5} s^{-1} and the dashed lines denote negative values of vorticity. The arrow A: positive vorticity; the arrow B: negative vorticity. Shaded area is shallower than 1200 m.

tides are the major constituents around the Kuril Islands, which interact nonlinearly, producing mainly a fortnightly tide (the linear fortnightly modulation is enhanced) and an M_2 tide although the dominant component remains the K_1 tidal current. Such nonlinear interactions between the components might cause difference in calculated transport. It remains a subject for future investigation.

Owing to the lack of current measurements, the reliability of the calculated current field is difficult to assess. We compare the model results with observation only in elevation data. Accordingly, although the results suggest that tidal exchange is a possible mechanism of water exchange through the Kuril Straits, we await future current measurements for comparison and improvement of our estimates of tidal exchange. Nevertheless, bidirectional mean currents in the Straits, through which these tidal exchanges are effectively produced, are consistent with the current structure observed in infrared images taken by *NOAA-12* and mentioned in the earlier work by Moroshkin (1966) and Leonov (1960). To emphasize this point, we have tracked numerous labeled particles in the calculated velocity field following earlier works (e.g., Miyama et al. 1995). Focusing on Bussol Strait, where most of the discharge is considered to occur, we performed 10 cycles of tracking from the ebb tide (Fig. 18). The calculated flow pattern of the Okhotsk Sea water (represented by blue particles in Fig. 18) has

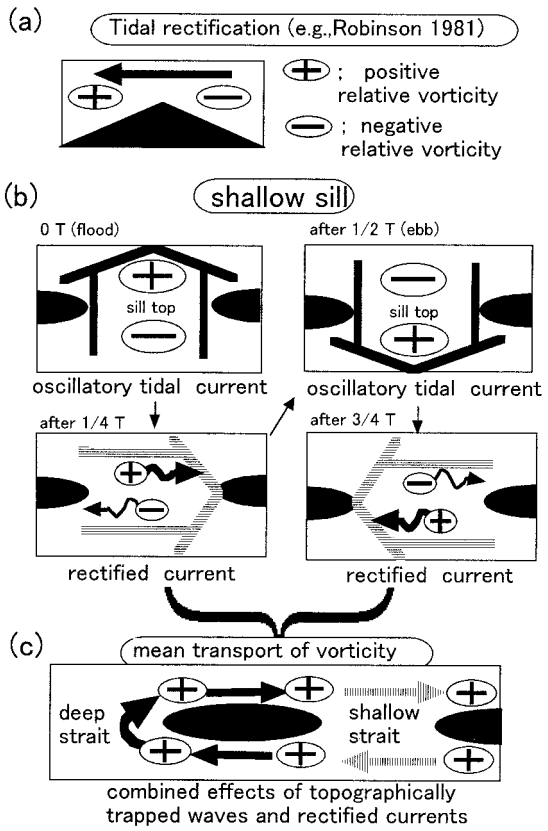

FIG. 16. Schematic illustration of the formation mechanism of mean vorticity by topographically trapped waves. (a) Vorticity generation by the stretching/squeezing effect. (b) Generation of a net flux of positive vorticity due to the combined effect of advection by the along-isobath current and the propagation of topographically trapped waves. (c) Net positive vorticity flux is conveyed by topographically trapped waves from a shallow strait to a deep strait where the waves can cross the sill, producing the mean bidirectional current structure.

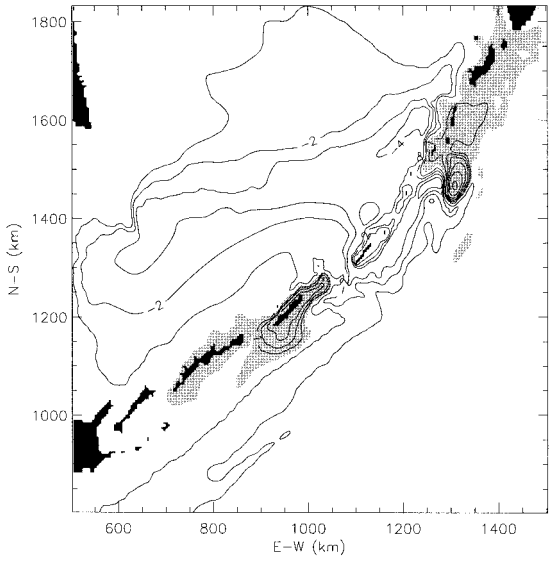

FIG. 17. Same as Fig. 9 but for the 2.5 km × 2.5 km grid sizes case and the contour unit of 0.8 Sv.

a qualitatively similar appearance to that of the infrared image. The simulation data in Fig. 18 exhibit such features as bidirectional and along-sill mean currents. Discharge from the middle of Bussol Strait is also visible, part of which joins the coastal side of the Oyashio current flowing offshore.

On the other hand, from geostrophic calculations based on CTD data, Kawasaki and Kono (1994) indicated that 1) outflows take place from Matsuwa Island to Kruzenshterna Strait and north of Simusir Island to Bussol Strait, 2) inflows take place from Nadezhdy Strait to Ketoy Island, and 3) strong vertical and horizontal mixing is caused at the northern straits and Bussol Strait by tidal currents, providing 2.9 Sv of Okhotsk Sea water and 2.5 Sv of mixed water, both of which join the Oyashio (12.8 Sv). Their results are different from our results in quantity, but the similarity in exchange and mixing locations with these observations suggests that their geostrophic calculation contains part of the tide-induced mean currents, which are in geostrophic balance. In fact, the presence of bidirectional currents is also observed by geostrophic calculation in Amchitka Strait (Reed 1990), which connects the Bering Sea and the North Pacific and is located north of the critical latitude for diurnal tides. This indicates the importance of direct current measurements for the estimation of water exchange between the two basins so that barotropic mean flow induced by subinertial tides can be precisely taken into account.

7. Summary

Our regional model has successfully reproduced the observed barotropic K_1 tidal field in the Okhotsk Sea, although the reliability of the calculated current field is difficult to assess owing to the lack of current measurements. Using the calculated tidal currents, the Eulerian mean outflow from the Okhotsk Sea is estimated to reach the significant value of 5.0 Sv for the K_1 tide, the main part of which is conducted through the Bussol, Kruzenshterna, and Chetverty Straits. In addition to the K_1 tide, the O_1, P_1, M_2, and S_2 tides induce Eulerian mean exchanges estimated at 3.5, 1.0, 0.3, and 0.1 Sv, respectively. These tidal exchanges are produced by bidirectional mean currents in the straits, consistent with the current structure observed in infrared images taken by *NOAA-12* and mentioned in the earlier work by Moroshkin (1966) and Leonov (1960). Therefore, it is suggested that tidal currents play an important role in water exchange between the Okhotsk Sea and the North Pacific, although confirmation of this prediction and improvements in accuracy await future observations.

We have shown that the mean currents are produced through the effects of topographically trapped waves as

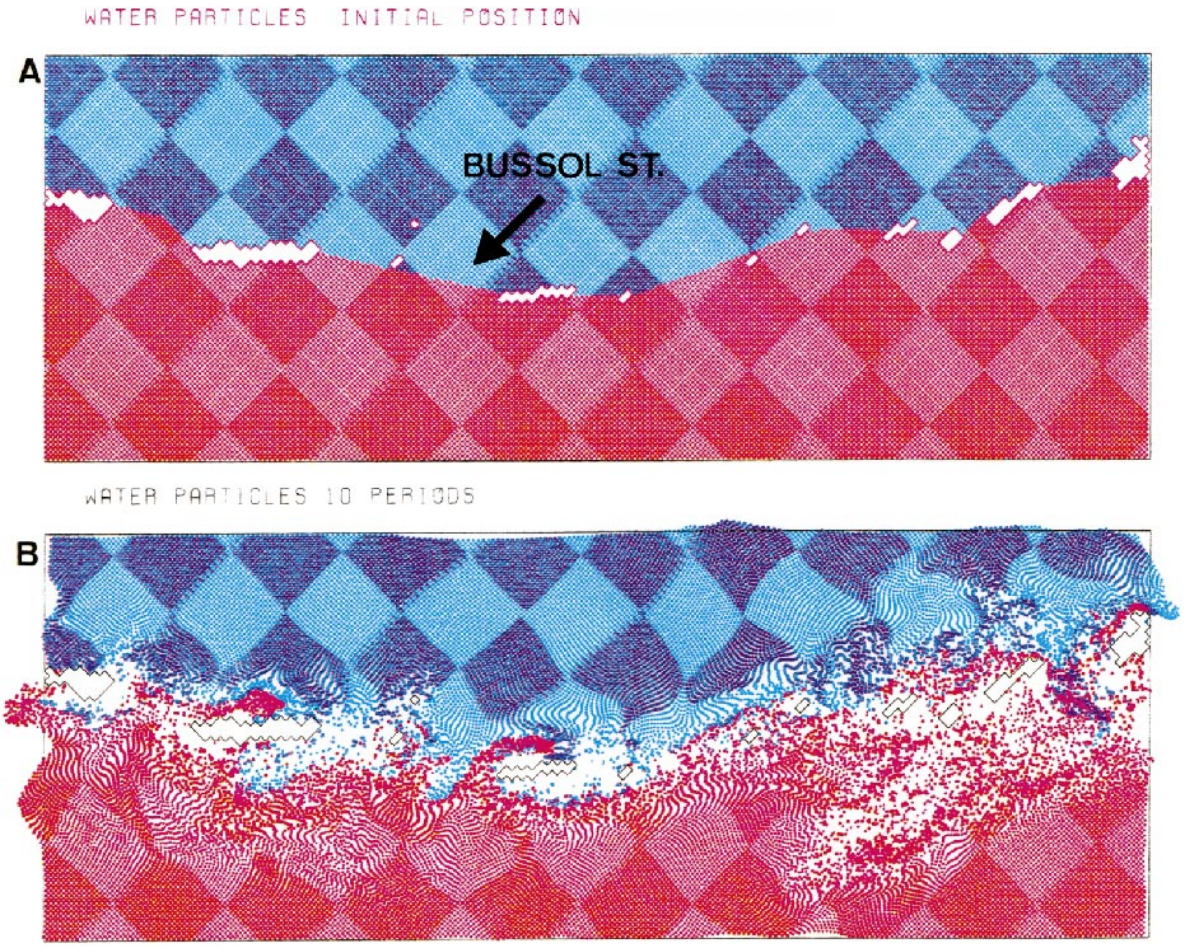

FIG. 18. Particle tracking results around the Kuril Straits, (a) initial position, and (b) after 10 cycles.

well as through well-known tidal rectification. In shallow straits (depth 200~600 m), tidal rectification mainly due to advection, vorticity generation by the stretching/squeezing effect, and damping by bottom friction produces the strong along-sill and weak bidirectional mean currents. On the other hand, in deep straits, such as Bussol strait, a net flux of positive vorticity from the adjacent shallow straits to the deep strait is caused by topographically trapped waves and produces strong bidirectional mean currents there. This net flux is caused by the fact that the along-isobath currents are in the same direction as the phase velocity of the topographically trapped waves with positive vorticity and are in the opposite direction to that with negative vorticity.

The mean currents produced by topographically trapped waves have three important properties: First, the mean currents induced by these waves are in near-geostrophic balance, since these waves are characterized as a rotational wave. Second, because this mechanism is responsible for the water exchange through deep straits, its depth makes the amount of the mean transport significant. In fact, roughly half of the total exchange induced by the K_1 tide is considered to be caused by the effect of topographically trapped waves. Last the mean exchanges induced by subinertial tides are much greater than those expected from the previous theories for tidal rectification which consider only the case of superinertial tides because superinertial tides are inefficient at generating topographically trapped waves. Thus, it is suggested that the energy of subinertial tides is effectively cascaded upscale to produce bidirectional mean exchange currents in geostrophic balance, causing significant water exchange between two basins even if they are separated by sills.

We have clarified the mechanisms of the horizontal exchange induced by the tidal currents which dominate the Kuril Straits region. However, since we use a depth-averaged model, the vertical structure is still unclear. Many observations indicate strong vertical mixing at the straits. Based on the vertical distributions of oxygen and density across Bussol Strait, Yasuoka (1967) suggested a surface layer inflow, a sinking outflow in the intermediate layer, and strong inflow over the sill. Tidal currents may also contribute significantly to vertical mixing and formation of the vertical circulation through the generation of internal waves, which are thought to

have a major influence on water modification, as discussed in the accompanying paper (Nakamura et al. 2000). Therefore, an investigation of the vertical structure of tidal currents around the straits, which includes the baroclinic effect, may be important for our understanding of the detailed transport processes and water mass transformation.

Besides tidal currents, water exchange and mixing can be caused by eddies (which often appear along the islands), flow driven by local winds, and advection and diffusion due to the difference in stratification between the Okhotsk Sea and the North Pacific. In particular, although exchange by the western boundary current of the subarctic gyre itself is of secondary importance as it flows along the Kuril Island Chain, this current can have a significant effect when it interacts with oscillating tidal currents. We should combine knowledge of the tidal currents with these effects in the future in order to identify and quantify the impact of the Okhotsk Sea upon the North Pacific.

Acknowledgments. We wish to acknowledge Prof. S. Saitoh (Hokkaido University, Japan) for the kind offer of *NOAA-12* AVHRR imagery. We also thank Dr. J. P. Matthews and anonymous reviewers for their critical reading and useful comments. Numerical Calculations were done on the FACOM M1800 and VP2600 at the Data Processing Center of Kyoto University.

REFERENCES

Awaji, T., N. Imasato, and K. Kunishi, 1980: Tidal exchange through a strait: A numerical experiment using a simple model basin. *J. Phys. Oceanogr.*, **10,** 1499–1508.

Chapman, D. C., 1989: Enhanced subinertial diurnal tides over isolated topographic features. *Deep-Sea Res.*, **36,** 815–824.

Chen, C., and R. C. Beardsley, 1995: A numerical study of stratified tidal rectification over finite-amplitude banks. Part I: Symmetric banks. *J. Phys. Oceanogr.*, **25,** 2090–2110.

Cushman-Roisin, B., 1994: *Introduction to Geophysical Fluid Dynamics.* Prentice-Hall, 320 pp.

Favorite, F., A. J. Dodimead, and K. Nasu, 1976: Oceanography of the Subarctic Pacific region: 1960–1971. *Int. North Pacific Fisheries Commission,* **33,** 1–187.

Haidvogel, D. B., A. Beckmann, D. C. Chapman, and R. Q. Lin, 1993: Numerical simulation of flow around a tall isolated seamount. Part II: Resonant generation of trapped waves. *J. Phys. Oceanogr.*, **23,** 2373–2391.

Hatayama, T., T. Awaji, and K. Akitomo, 1996: Tidal currents in the Indonesian Seas and their effect on transport and mixing. *J. Geophys. Res.*, **101,** 12 353–12 373.

Holton, J. R., 1979: *An Introduction to Dynamic Meteorology.* 2d ed. Academic Press, 391 pp.

Huthnance, J. M., 1973: Tidal current asymmetries over the Norfolk Sandbank. *Estuar. Coastal Mar. Sci.*, **1,** 89–99.

——, 1981: On mass transports generated by tides and long waves. *J. Fluid Mech.,* **102,** 367–387.

Kawasaki, Y., and T. Kono, 1992: Baroclinic water exchange in the Kuril Basin and the northwestern Pacific in summer (in Japanese). *Sea and Sky,* **68,** 41–54.

——, and ——, 1994: Distribution and transport of Subarctic Waters around the middle of Kuril Islands (in Japanese). *Sea and Sky,* **70,** 71–84.

Kitani, K., 1973: An oceanographic study of the Okhotsk Sea—Particularly in regard to cold waters. *Bull. Far Seas Fish. Res. Lab.,* **9,** 45–77.

Kowalik, Z., and A. Yu. Proshutinsky, 1995: Topographic enhancement of tidal motion in the western Barents Sea. *J. Geophys. Res.,* **100,** 2613–2637.

——, and I. Polyakov, 1998: Tides in the Sea of Okhotsk. *J. Phys. Oceanogr.,* **28,** 1389–1409.

LeBlond, P. H., and L. A. Mysak, 1978: *Waves in the Ocean.* Elsevier Scientific, 602 pp.

Leonov, A. K., 1960: The Sea of Okhotsk. National Technical Information Service, Springfield, VA.

Longuet-Higgins, M. S., 1965: Some dynamical aspects of ocean currents. *Quart. J. Roy. Meteor. Soc.,* **91,** 425–457.

Mazzega, P., and M. Bergé, 1994: Ocean tides in the Asian semienclosed seas from TOPEX/POSEIDON. *J. Geophys. Res.,* **99,** 24 867–24 881.

Miyama, T., T. Awaji, K. Akitomo, and N. Imasato, 1995: Study of seasonal transport variations in the Indonesian Seas. *J. Geophys. Res.,* **100,** 20 517–20 541.

Moroshkin, K. V., 1966: Water masses of the Sea of Okhotsk. U.S. Dept. of Commerce Joint Publication Research Service 43, 942, 98 pp.

Nakamura, T., T. Awaji, T. Hatayama, K. Akitomo, T. Takizawa, T. Kono, Y. Kawasaki, and M. Fukazawa, 2000: The generation of large-amplitude unsteady lee waves by subinertial K_1 tidal flow: A possible vertical mixing mechanism in the Kuril Straits. *J. Phys. Oceanogr.,* **30,** 1601–1621.

Odamaki, M., 1994: Tides and tidal currents along the Okhotsk coast of Hokkaido. *J. Oceanogr.,* **55,** 265–279.

Ogura, S., 1923: Tides in the Sea of Okhotsk (in Japanese). *Suiro Zasso,* **10** (274), 71–88.

Orlanski, I., 1976: A simple boundary condition for unbounded hyperbolic flows. *J. Comput. Phys.,* **21,** 251–269.

Reed, R. K., 1990: A year-long observation of water exchange between the North Pacific and the Bering Sea. *Limnol. Oceanogr.,* **35** (7), 1604–1609.

Reid, J. L., 1965: *Intermediate Waters of the Pacific Ocean.* Johns Hopkins Press, 85 pp.

Ridderinkhof, H., 1989: Tidal and residual flows in the Western Dutch Wadden Sea: Vorticity balances. *Neth. J. Sea Res.,* **24,** 9–16.

Robinson, I. S., 1981: Tidal vorticity and residual circulation. *Deep-Sea Res.,* **28A,** 195–212.

Schwiderski, E. W., 1979: Global Ocean Tides, II: The semidiurnal principal lunar tide (M_2). *Atlas of Tidal Charts and Maps,* Naval Surface Weapons Center.

——, 1980: On charting global ocean tides. *Rev. Geophys.,* **18,** 243–268.

——, 1981: Global Ocean Tides, IV: The diurnal luni-solar declination tide (K_1). *Atlas of Tidal Charts and Maps,* Naval Surface Weapons Center.

Stabeno, P. J., R. K. Reed, and J. E. Overland, 1994: Lagrangian measurements in the Kamchatka Current and Oyashio. *J. Oceanogr.,* **50,** 653–662.

Suzuki, K., and S. Kanari, 1986: Tides in the Sea of Okhotsk (in Japanese). *Oceanogr. Mag.,* **18,** 455–463.

Talley, L. D., 1991: An Okhotsk Sea water anomaly: Implications for ventilation in the North Pacific. *Deep-Sea Res.,* **38,** 171–190.

——, 1993: Distribution and formation of North Pacific Intermediate Water. *J. Phys. Oceanogr.,* **23,** 517–537.

Thomson, R. E., P. H. LeBlond, and A. B. Rabinovich, 1997: Oceanic odyssey of a satellite-tracked drifter: North Pacific variability delineated by a single drifter trajectory. *J. Oceanogr.,* **53,** 81–87.

Warner, M. J., J. L. Bullister, D. P. Wisegraver, R. H. Gammon, and R. F. Weiss, 1996: Basin-wide distributions of chlorofluorocarbons CFC-11 and CFC-12 in the North Pacific. *J. Geophys. Res.,* **101,** 20 525–20 542.

Wüst, G., 1930: Meridionale Schichtung und Tiefenzirkulation in der Westhalften der drei Ozeane. *J Cons. Int. l'Explor. Mer,* **5,** 21 pp.

Yasuda, I., 1997: The origin of the North Pacific intermediate water. *J. Geophys. Res.*, **102,** 893–910.

——, K. Okuda, and Y. Shimizu, 1996: Distribution and formation of North Pacific Intermediate Water in the Kuroshio–Oyashio interfrontal zone. *J. Phys. Oceanogr.*, **26,** 448–465.

Yasuoka, T., 1967: Hydrography in the Okhotsk Sea—(1). *Oceanogr. Mag.*, **19,** 61–72.

Zimmerman, J. T. F., 1978: Topographic generation of residual circulation by oscillatory (tidal) currents. *Geophys. Astrophys. Fluid Dyn.*, **11,** 35–47.